Technical Report

TR-10-62

Evaluation of low-pH cement degradation in tunnel plugs and bottom plate systems in the frame of SR-Site

Fidel Grandia, Juan-Manuel Galíndez,
Jorge Molinero, David Arcos

Amphos [21]

September 2010

Svensk Kärnbränslehantering AB
Swedish Nuclear Fuel
and Waste Management Co

Box 250, SE-101 24 Stockholm
Phone +46 8 459 84 00

ISSN 1404-0344
SKB TR-10-62

Evaluation of low-pH cement degradation in tunnel plugs and bottom plate systems in the frame of SR-Site

Fidel Grandia, Juan-Manuel Galíndez,
Jorge Molinero, David Arcos

Amphos [21]

September 2010

Keywords: SKBdoc 1259182, Low pH cement, Plug, Backfill, Bottom plate.

This report concerns a study which was conducted for SKB. The conclusions and viewpoints presented in the report are those of the authors. SKB may draw modified conclusions, based on additional literature sources and/or expert opinions.

A pdf version of this document can be downloaded from www.skb.se.

Abstract

Low-pH concrete plugs are going to be used during the backfilling of depositional tunnels of the high-level nuclear waste repository. The stability of these plugs, however, is thought to be affected by water-concrete interaction that may lead to cement degradation and dissolution. Alkaline plumes derived from such a degradation could jeopardize the chemical stability of the clay material in the backfill due to the enhanced dissolution kinetics under high-pH solutions.

In this study, the cement durability of concrete plugs to be used in the repository is numerically evaluated by performing reactive transport simulations based on the geochemical degradation of the cement compounds, mainly calcium silicate hydrates (CSH). The implementation of degradation process into the geochemical model is based on a solid solution approach for CSH alteration. The numerical model also takes into account the dependency of transport properties (e.g. molecular diffusion coefficient) with the changes in porosity due to mineral precipitation-dissolution. The simulations predict that the effect of low-pH concrete alteration on the stability of backfill materials would be low. The main process governing geochemistry in the backfill-concrete boundary would be the quick loss of porosity due to ettringite precipitation. The very high molar volume of this mineral enhances the rate of clogging. The ettringite formation is mainly driven by the high sulphate concentration in the backfill porewater, which in turn is controlled by the equilibrium with gypsum in the backfill. The release and diffusion of calcium (from CSH replacement) and Al (from katoite dissolution) from concrete causes ettringite precipitation at the concrete-backfill boundary. The loss of porosity dramatically reduces solute diffusion and, consequently, the backfill-concrete system remains almost invariably for hundreds of years.

Sammanfattning

Pluggar av låg-pH betong kommer att användas under återfyllningen av deponeringstunnlarna i kärnbränsleförvaret. Stabiliteten av pluggarna påverkas av interaktion med grundvattnet, vilket kan leda till nedbrytning och upplösning av cementen. Den alkaliska plymen från upplösningen skulle kunna påverka den kemiska stabiliteten hos lermaterialet i återfyllningen på grund av ökad upplösningshastighet under alkaliska förhållanden.

In den här studien har stabiliteten hos cementfasen de betongpluggar som skall användas i förvaret utvärderats numeriskt med reaktiv-transport simuleringar baserade på den geokemiska nedbrytningen av cementkomponenterna, framförallt kalcium-silikat-hydraten (CSH). Implementeringen av degraderingsprocessen i den geokemiska modellen är baserad på en fast-lösning beskrivning av CSH-omvandling. Den numeriska modellen hanterar också beroendet mellan transportparametrarna (t ex diffusionskoefficenter) och förändringar i porositet orsakad av upplösnings/utfällningsreaktioner. Simuleringarna indikerar att effekten från omvandling av låg-pH cement på återfyllningsmaterialets stabilitet blir liten. Den styrande processen för geokemin i gränsområdet mellan återfyllning och betong är den snabba porositetsminskning som orsakas av ettringitutfällning. Detta minerals stora molvolym ger en snabb tilltäppning av porsystemet. Etteringiten bildas från de höga sulfathalterna i återfyllningens porvatten, vilka kontrolleras av jämvikten med gips i materialet. Frigörelsen och transporten av kalcium (från CSH omvandling) och aluminium (från upplösning av kaotit) från betong orsakar ettringitutfällning i gränsskiktet mellan betong och återfyllning. Förlusten av porositet minskar diffusionen av specier radikalt och som en konsekvens av detta blir systemet i praktiken stabilt för hundratals år.

Contents

1 Introduction

Backfilling of depositional tunnels is expected to be complicated by the inflowing waters from granite rocks in two ways: (1) erosion and transport of backfill material out of the depositional tunnel, and (2) expansion due to swelling of clay components of the backfill, making it physically unstable. To keep the backfill in place, low-pH concrete plugs are included since they provide physical restraint (Figure 1-1).

Along the post-operational phase, the plug will limit water flow from the deposition tunnel past the plug to such an extent that no harmful backfill erosion takes place out from the deposition tunnel. The stability of concrete plugs, however, is though to be affected by water-concrete interaction that may lead to concrete degradation and dissolution. In addition, alkaline plumes derived from such a degradation could jeopardize the chemical stability of the clay material in the backfill due to the enhanced dissolution kinetics under high-pH solutions.

In the SKB repository design the use of low-pH concrete is envisaged in different situations. In two sub-systems, it will be used as structural material in the tunnel plug and in the bottom plate.

The main objective of this project is to assess the concrete durability in concrete plugs under inflowing water conditions. Such a durability depends basically on the geochemical degradation of the cement compounds, mainly calcium silicate hydrates (CSH), whose dissolution can result in porosity increase and leading to changes in the hydraulic properties (e.g. permeability). In turn, these changes can speed up the degradation process and the groundwater flux into the system. A second objective is the calculation of the extent of the alkaline plume into the backfill as a result of CSH dissolution to evaluate the potential effect on the clay material.

Since the processes of interest in the project need to be evaluated in a hydrodynamic setting, reactive transport modelling is required. The numerical simulations, in addition, must include the coupled changes between dissolution/precipitation of minerals and hydraulics. The approach followed in the project consists of three steps:

1) Simulation of low-pH concrete composition and porosity.
2) Definition of model domains and geochemical approach.
3) Numerical simulation of low-pH concrete degradation.

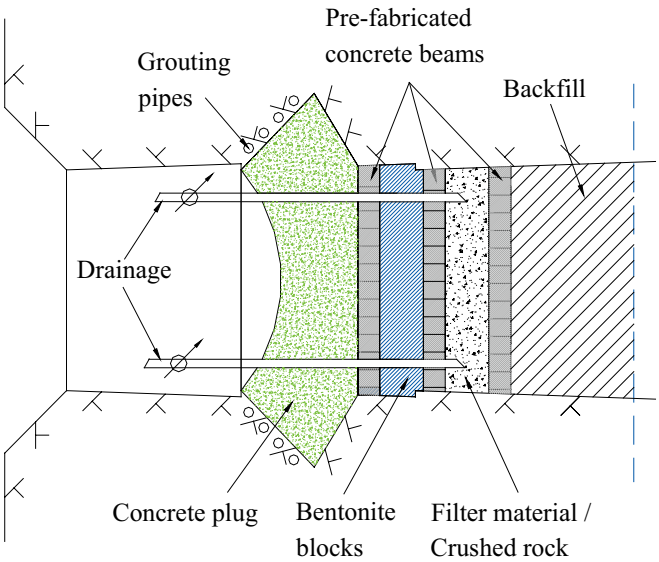

Figure 1-1. *Sketch of the section of a tunnel plug in a HLNW repository with the location of the concrete plug.*

In the first step, the mineral composition of the initial cement paste used for the plug is calculated using CEMHYD3D /Bentz 2000/ that is a set of computer programs able to simulate the hydration and microstructure development of a three-dimensional arrangement of multi-size, multi-phase cement particles. The results of this simulation provide initial conditions of the reactive transport models used to simulate the low-pH concrete degradation.

In the second step the physical features of the modelled domain are defined and justified. Although the repository will be located in rock mass of good quality with mostly relatively low fracturing, it can not be disregarded that a hydraulic conductive fracture can be intersected by the low-pH concrete in the tunnel plug. The rate of alteration of low-pH concrete is expected to be substantially higher where conductive fractures meet the tunnel plug or bottom plate sub-systems, compared with direct granite-concrete contacts.

Also, this second part of the project includes the assessment of the geochemical approach to be adopted for the cement compounds. The model prediction of the concrete alteration is challenging mainly due to the progressive change in composition of the CSH compounds as the alteration proceeds (incongruent dissolution-precipitation). This requires the use of solid solution approaches and the consideration of dissolution-precipitation as kinetic processes. Following /Grandia et al. 2010/, the approach adopted is the solid solution model by /Sugiyama and Fujita 2006/.

The reactive transport calculations are performed in the third part of the project.

2 Definition of model domain and geochemical approach

2.1 Model domain and spatial discretisation

The selected model domain for the reactive transport simulations is one-dimensional and reproduces the contact between the major rock types and engineered material in Figure 1-1: (1) the backfill, (2) the concrete plug, and (3) the host granite rock (Figure 2-1). Other minor elements in between (filters, watertight seal, pipes, concrete beams, …) are not considered since their role in the solute transport and reactivity is not so relevant as the major domains and, in general, they share a similar rock composition (e.g. bentonite watertight seal is envisaged to be close to backfill in terms of composition).

Granite in the model is not considered physically as a rock. Instead, a flowing groundwater of granitic, Forsmark-type composition is considered. The reason behind this selection is the stable mineralogy of the granite mineralogy which is not expected to undergo significant changes in spite of the diffusion of alkaline fluids from concrete alteration. Moreover, the model results by /Grandia et al. 2010/ show that the alteration front in the granite-concrete interface does not progress much through time, and the geochemical influence to the backfill-concrete contact located at 0.5 m is though to be negligible. This relative low affectation of concrete is predicted even assuming an "aggressive" (conservative) chemical condition for granite fluids and the concrete (i.e. a fixed composition boundary condition).

The more relevant outcome from the modelling in this project is the interaction between backfill and concrete since it can provide clues for the mechanical stability of the engineered barrier system. The diffusion of solutes (mainly calcium) from the backfill porewater to the concrete is believed to play a role in the rate of degradation of concrete since cement compound alteration is essentially a decalcification process. On the other hand, the diffusion of OH^- from concrete porewater may enhance the solubility of clay compounds jeopardising the mechanical properties of the backfill.

The evidence that major geochemical changes are predicted to occur in the material interfaces lead to design a model grid with a much finer discretisation in these contacts, with length increments of as low as 1 mm (Table 2-1).

The permeability of both backfill and concrete materials are very low so that the solute transport is basically driven by diffusion (i.e. by concentration gradients).

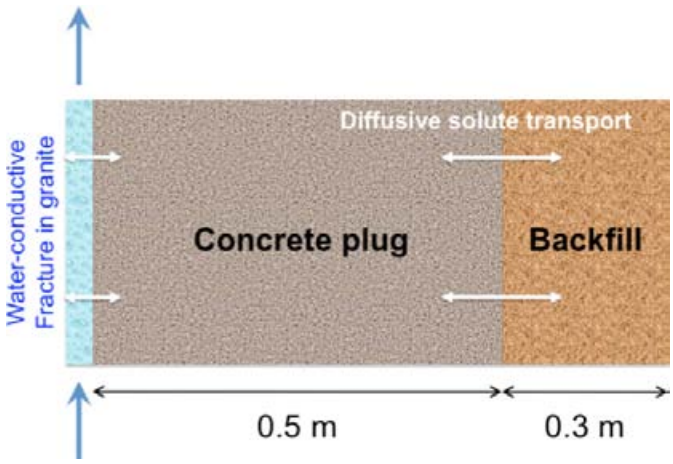

Figure 2-1. *Domain selected in the reactive transport simulations.*

Table 2-1. Spatial discretisation of the modelled domain.

	nº elements	ΔX (m)	Total X (m)
backfill boundary	1	0.1	0.1
backfill	20	0.01	0.2
backfill-concrete transition	10	0.001	0.01
concrete	20	0.001	0.02
concrete	46	0.01	0.46
concrete	20	0.001	0.02
groundwater (granite)	1	0.01	0.01

2.2 Geochemical approach: Concrete degradation and solid solution model

The alteration of the cementitious materials performed in laboratory shows a dependence between the pH of pore water and the Ca-Si ratio of the hydrated calcium-silicate (CSH) phases /Flint and Wells 1934, Taylor 1950, Kalousek 1952, Greenberg and Chang 1965, Fujii and Kondo 1981, Harris et al. 2002, Chen et al. 2004, and many others/. The Ca-Si ratio decreases as the CSH is progressively replaced by Si-richer phases denoting a clear incongruent CSH dissolution. In the initial stages, the concrete alteration is limited to portlandite dissolution as pure phase or as a $Ca(OH)_2$ hypothetical end-member of CSH phases. In the latter case, the loss of calcium results in the formation of new CSH with lower Ca/Si ratio. The precise chemistry of these CSH formed during this evolution is not clear because of their gel-like nature.

In the experiments dealing with low-pH samples (initial Ca/Si ratios between 0.7 and 1.2) some differences are observed in experimental datasets reported in literature. A sharp and sudden drop in pH coupled with an almost stable Ca/Si is reported, as an example, by /Harris et al. 2002/ (Figure 2-2). Milder variations are, in contrast, provided by /Flint and Wells 1934, Greenberg and Chang 1965 and Chen et al. 2004/.

The incongruent dissolution of Ca-rich solids leads to an increase in the calcium concentration in solution at the beginning of the alteration process (Figure 2-3). In time, the [Ca] concentration

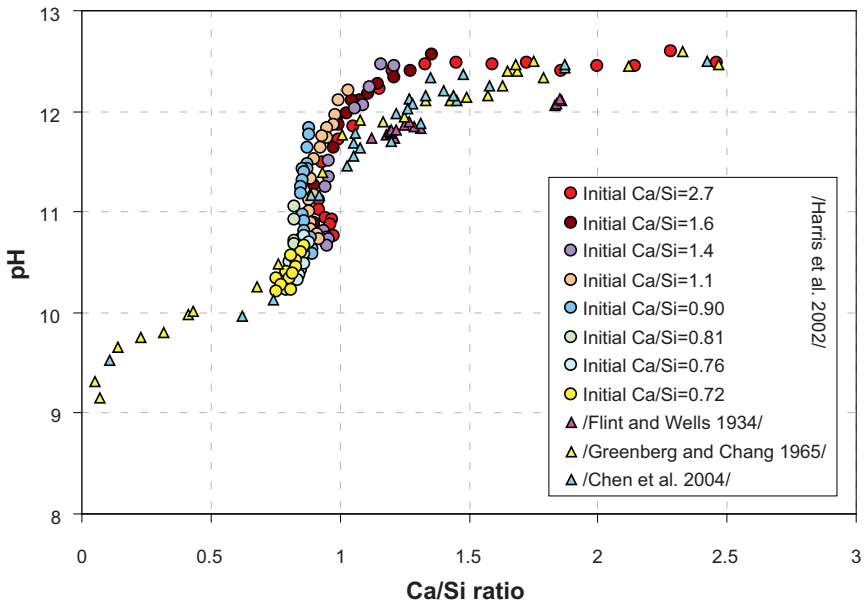

Figure 2-2. *Evolution of the CSH composition vs. pH reported from the experiments by /Harris et al. 2002, Flint and Wells 1934, Greenberg and Chang 1965, Chen et al. 2004/. Note the different shape of the curve at Ca/Si ratio from 0.7 to 1.2.*

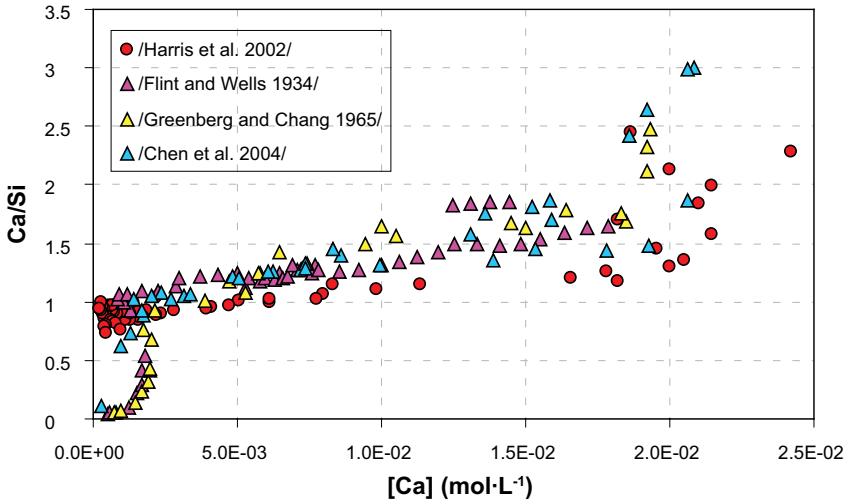

Figure 2-3. *Evolution of the CSH composition vs. $[Ca]_T$ reported from the experiments by /Harris et al. 2002, Flint and Wells 1934, Greenberg and Chang 1965 and Chen et al. 2004/.*

decreases reflecting the equilibrium with Ca-poor CSH phases. Part of this calcium can be precipitated back as calcite and/or ettringite if the concentration of aqueous C(IV) and sulphate species is high enough. The concentration of silicon shows an opposite behaviour, increasing through time (Figure 2-4). As pH decreases, silica saturation can be achieved and, consequently, part of the Si goes back to the solid phase.

The consideration of CSH as a solid solutions has recently been used to model CSH degradation /Berner 1988 and 1992, Kersten 1996, Börjesson et al. 1997, Rahman et al. 1999, Kulik and Kersten 2001, Sugiyama and Fujita 2006, Carey and Lichtner 2007, Walker et al. 2007, Small and Thompson 2008/. This approach is a geochemical artefact since CSH phases are not solid solutions because they are not crystalline solids, which is an imperative requirement for a solid solution. In addition, crystalline equivalents of CSH are not proved to be solid solutions. Nevertheless, this consideration is an elegant and accurate way to numerically model an incongruent dissolution.

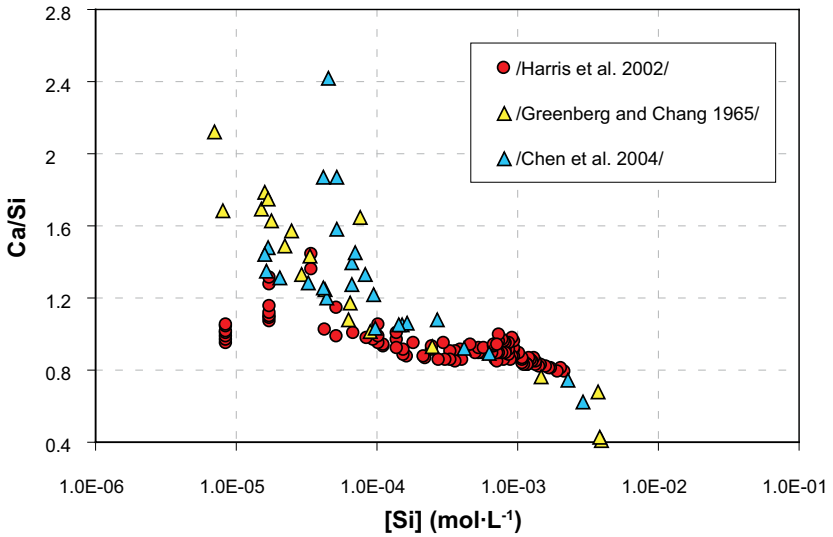

Figure 2-4. *Evolution of the CSH composition vs. $[Si]_T$ reported from the experiments by /Harris et al. 2002, Greenberg and Chang 1965, and Chen et al. 2004/.*

Most of them assumed a strong non-ideality of the solid solution series (meaning that the solubility constant of a CSH member is depending not only in its molar fraction but also in the composition of the solid itself:

$$K_{ss}(x_{ss}) = \left(K_1 \lambda_1 x_{ss}\right)^{x_{ss}} \left(K_2 \lambda_2 (1 - x_{ss})\right)^{1-x_{ss}}$$

where K_1 and K_2 are the solubility constants of the end-members, x is the molar fraction of the CSH solid. λ_1 and λ_2 are activity constants that govern the non-ideality of the system and can be treated mathematically by means of the Guggenheim expressions (for a development of a model with 3 terms) as follows:

$$\ln \lambda_1 = (1-x_1)^2[\alpha_0+\alpha_1(4x_1-1)+(2x_1-1)(\alpha_2(6x_1-1)+\alpha_3(16x_1^2-10x_1+1))]$$

$$\ln \lambda_2 = x_1^2\,[\alpha_0+\alpha_1(4x_1-3)+(2x_1-1)(\alpha_2(6x_1-5)+\alpha_3(16x_1^2-22x_1+7))]$$

where $\alpha_0, \ldots, \alpha_n$ are the interaction parameters.

2.2.1 The Sugiyama and Fujita approach

In a recent modelling study, /Grandia et al. 2010/ showed that the solid solution approach by /Sugiyama and Fujita 2006/ was valid to reproduce experimental data of CSH degradation. This approach uses two solid solution end-members (SiO_2 and portlandite) and the conditional solubility constants for the intermediate members as a function of the Ca/Si ratio of the solid solution is calculated following the next equalities:

(1) For $0<Ca/Si_{CSH}\leq 0.461$:

$$\log K_S = \log\left[K_{So} \cdot \left\{\frac{1}{(Ca/Si)+1}\right\}\right]$$

$$\log K_C = \frac{(Ca/Si)}{1+(Ca/Si)} \cdot \log K_{Co} - \frac{(Ca/Si)}{1+(Ca/Si)} \cdot \log\left(\frac{(Ca/Si)}{1+(Ca/Si)}\right) + \left[\frac{(Ca/Si)}{\{1+(Ca/Si)\}^2}\right] \cdot$$

$$\left[37.019 + 36.724 \cdot \left\{\frac{(Ca/Si)-1}{1+(Ca/Si)}\right\} + 164.17 \cdot \left\{\frac{(Ca/Si)-1}{1+(Ca/Si)}\right\}^2\right]$$

(2) For $0.461<Ca/Si_{CSH}\leq 0.833$:

$$\log K_S = \frac{1}{1+(Ca/Si)} \cdot \log K_{So} - \frac{1}{1+(Ca/Si)} \cdot \log\left(\frac{1}{1+(Ca/Si)}\right) + \left[\frac{(Ca/Si)}{\{1+(Ca/Si)\}^2}\right] \cdot$$

$$\left[-18.623 + 57.754 \cdot \left\{\frac{1-(Ca/Si)}{1+(Ca/Si)}\right\} - 58.241 \cdot \left\{\frac{1-(Ca/Si)}{1+(Ca/Si)}\right\}^2\right]$$

$$\log K_C = \frac{(Ca/Si)}{1+(Ca/Si)} \cdot \log K_{Co} - \frac{(Ca/Si)}{1+(Ca/Si)} \cdot \log\left(\frac{(Ca/Si)}{1+(Ca/Si)}\right) + \left[\frac{(Ca/Si)}{\{1+(Ca/Si)\}^2}\right] \cdot$$

$$\left[37.019 + 36.724 \cdot \left\{\frac{(Ca/Si)-1}{1+(Ca/Si)}\right\} + 164.17 \cdot \left\{\frac{(Ca/Si)-1}{1+(Ca/Si)}\right\}^2\right]$$

(3) For $0.833 < Ca/Si_{CSH} \leq 1.755$:

$$\log K_S = \frac{1}{1+(Ca/Si)} \cdot \log K_{So} - \frac{1}{1+(Ca/Si)} \cdot \log\left(\frac{1}{1+(Ca/Si)}\right) + \left[\frac{(Ca/Si)}{\{1+(Ca/Si)\}^2}\right] \cdot$$

$$\left[-18.656 + 49.712 \cdot \left\{\frac{1-(Ca/Si)}{1+(Ca/Si)}\right\} + 25.033 \cdot \left\{\frac{1-(Ca/Si)}{1+(Ca/Si)}\right\}^2\right]$$

$$\log K_C = \frac{(Ca/Si)}{1+(Ca/Si)} \cdot \log K_{Co} - \frac{(Ca/Si)}{1+(Ca/Si)} \cdot \log\left(\frac{(Ca/Si)}{1+(Ca/Si)}\right) + \left[\frac{(Ca/Si)}{\{1+(Ca/Si)\}^2}\right] \cdot$$

$$\left[36.937 + 7.8302 \cdot \left\{\frac{(Ca/Si)-1}{1+(Ca/Si)}\right\} - 50.792 \cdot \left\{\frac{(Ca/Si)-1}{1+(Ca/Si)}\right\}^2\right]$$

(4) For $1.755 < Ca/Si_{CSH}$:

$\log K_s = -7.853$

$\log K_c = 22.81$

In all cases, $log\ K_{So}$ and $log\ K_{Co}$ are the solubility constants for SiO_2 and portlandite respectively.

$SiO_2(am) \leftrightarrow SiO_2(aq)$ $\qquad$ $log\ K_{So} = -2.71$

$Ca(OH)_2 + 2H^+ \leftrightarrow Ca^{2+} + 2H_2O$ $\qquad$ $log\ K_{Co} = 22.81$

$log\ K_S$ and $log\ K_C$ are the calculated conditional solubility products of both end members in the solid solution.

Once K_S and K_C for each solid solution is calculated, the K_{CSH} can be obtained using:

$$K_{ss}(x_{ss}) = (K_S \cdot x_{ss})^{x_{ss}} (K_C \cdot (1-x_{ss}))^{1-x_{ss}}$$

Table 2-2 and Figure 2-5 show the corresponding K_{CSH} as a function of the Ca/Si ratio of the CSH.

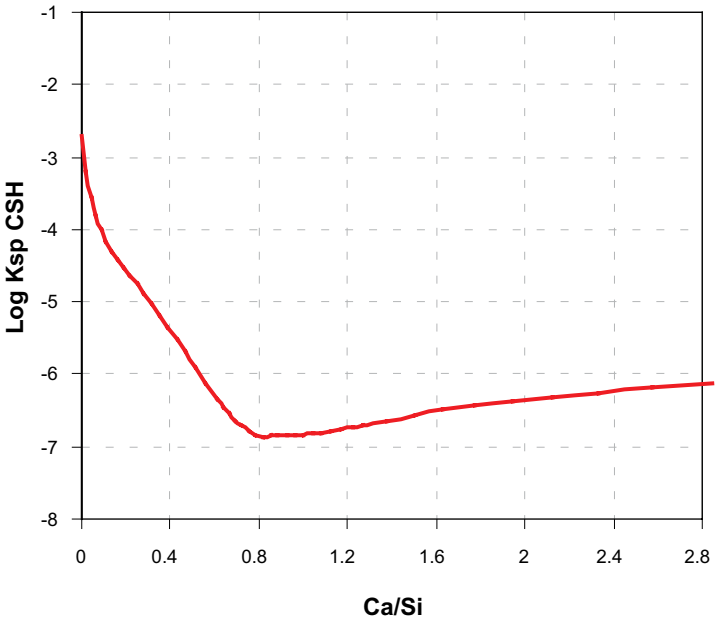

Figure 2-5. *$log\ K_{CSH}$ as a function of the Ca/Si ratio calculated using the /Sugiyama and Fujita 2006/ approach.*

Table 2-2. Composition of the calcium-silicate hydrate phases considered in the model using the /Sugiyama and Fujita 2006/ approach, and the corresponding solubility constants.

CSH	X_{Si}	Ca/Si	log K
CSH_285	0.26	2.85	–6.13
CSH_257	0.28	2.57	–6.19
CSH_233	0.30	2.33	–6.25
CSH_212	0.32	2.12	–6.31
CSH_194	0.34	1.94	–6.38
CSH_178	0.36	1.78	–6.43
CSH_163	0.38	1.63	–6.50
CSH_150	0.40	1.50	–6.57
CSH_138	0.42	1.38	–6.64
CSH_127	0.44	1.27	–6.71
CSH_122	0.45	1.22	–6.74
CSH_117	0.46	1.17	–6.77
CSH_113	0.47	1.13	–6.79
CSH_108	0.48	1.08	–6.81
CSH_104	0.49	1.04	–6.83
CSH_100	0.50	1.00	–6.84
CSH_096	0.51	0.96	–6.85
CSH_092	0.52	0.92	–6.85
CSH_089	0.53	0.89	–6.84
CSH_085	0.54	0.85	–6.83
CSH_081	0.55	0.81	–6.83
CSH_079	0.56	0.79	–6.83
CSH_075	0.57	0.75	–6.78
CSH_072	0.58	0.72	–6.72
CSH_070	0.59	0.70	–6.64
CSH_067	0.60	0.67	–6.55
CSH_064	0.61	0.64	–6.45
CSH_061	0.62	0.61	–6.35
CSH_056	0.64	0.56	–6.13
CSH_051	0.66	0.51	–5.90

3 Simulation of the microstructure of concrete

3.1 Introduction

In this section, the mineralogical and physical features of the concrete to be used in the construction of a plug in deposition tunnels in the KBS-3 repository is calculated. From the concrete recipe provided by the manufacturer, the composition and porosity of the hydrated cement is obtained simulating thus the hydration process. The results from this calculation is the basis for subsequent reactive transport simulations.

3.2 Materials

The mixture for concrete involves the materials listed in Table 3-1. They include Cement I 42.5 MH/LA/SR (Anläggningscement by Cementa AB), which is adapted for solid constructions with demands for moderate heat development, if there is a risk of alkali–silica reactions and if there is a demand for higher sulphate resistance. The characteristic PSD curve was found in /du Plessis et al. 2007/.

The chemical composition of Cement I 42.5 MH/LA/SR is shown in Table 3-2, in which all components are expressed in weight percentages.

3.3 Methodology and calculations using CEMHYD3D

The initial composition of the hydrated paste is determined following successive steps: (1) calculation of the particle size distribution of the initial microstructure, (2) distribution of cement phases, and (3) simulation of hydration process. This methodology provides a rational framework to obtain the likely constitution of concrete whatever the conditions of hydration (and actually any data other than the volume fractions involved in the un-hydrated mixture). Although a relatively large uncertainty still exists in the actual evolution of the process of hydration under field conditions, this method will be able to define reasonable starting points for subsequent modelling of degradation.

The tools provided by the Virtual Cement and Concrete Testing Laboratory (VCCTL; http://ciks.cbt.nist.gov) have been used in order to set up the initial state of cement concrete. The underlying software package of the VCCTL, namely CEMHYD3D, is described in /Bentz et al. 1994/ and was intensively tested in numerous applications /Bentz 1997, Bentz and Heacker 1999, Bentz et al. 1999, Bentz et al. 2000, Bentz and Conway 2001/.

3.3.1 Creation of the particle size distribution and generation of the initial microstructure

Following the volume fraction of each component, a three dimensional image of the mixture is calculated (Table 3-3). The volume considered was 100 μm×100 μm×100 μm volume, where 1 pixel in the image is equivalent to 1 μm.

The number of cement, and silica fume, particles of each diameter to be placed in the initial three-dimensional microstructure is specified in accordance to their corresponding particle size distribution (i.e. the mass fraction expressed as a function of particle diameter). Table 3-4 shows the calculations done for that purpose. Silica fume was assumed to be composed of microsilica particles with uniform diameter of 1 μm. The resulting number of particles obtained is listed in the column labelled “Number of particles”.

The calculated 3D cement-based concrete mixture microstructure consists of the sum of the selected components in water, namely cement clinker and silica fume, with their respective particle size distribution. The influence of the superplasticizer can also be modelled in a two-fold way: (1) by enabling the flocculation into several flocs, and (2) by ‘dispersing’ the particles into the initial microstructure. Details of the process can be found in the User’s Guide of CEMHYD3D /Bullard 2000/.

Table 3-1. Concrete recipe.

Component	Weight (kg)
Water	165.00
Cement I 42.5 MH/LA/SR	120.00
Silica fume (densified)	80.00
Limestone filler	369.00
Sand (0 – 8 mm)	1,037.00
Gravel (8 – 16 mm)	558.00
Superplasticizer	6.38
Total	2,335.38

Table 3-2. Chemical composition of Cement I 42.5 MH/LA/SR, which is the main component of the concrete plug.

Component	Weight%
CaO	62.50
SiO_2	21.00
Al_2O_3	6.50
Fe_2O_3	2.50
SO_3	2.00
MgO	2.00
Others	3.50

Table 3-3. Volume fraction of the components of the cement paste of concrete.

Component	Weight (kg)	Specific gravity	Volume (dm^3)	Number of pixels
Water	684.23	1.00	684.23	684,229
Cement I 42.5 MH/LA/SR	497.62	3.20	155.51	155,507
Silica fume	331.75	2.07	160.26	160,264
Superplasticizer	26.46	–	–	–
Total	1,540.05	–	1,000.00	1,000,000

Table 3-4. Calculations for the assignment of pixels to each component.

	Radius (µm)	Diameter (µm)	Individual Volume (µm³)	Mass fraction	Number	Number fraction	Number of pixels	Number of particles
Cement 42.5 MH/LA/SR	0	1	1	0.075072	0.075072	0.837220	130,193	130,193
	1	3	19	0.145221	0.007643	0.085239	13,255	698
	2	5	81	0.203852	0.002517	0.028067	4,364	54
	3	7	179	0.262421	0.001466	0.016350	2,542	14
	4	9	389	0.316872	0.000815	0.009084	1,412	4
	5	11	739	0.374798	0.000507	0.005656	879	1
	6	13	1189	0.422756	0.000356	0.003965	616	1
	7	15	1791	0.462653	0.000258	0.002881	447	0
	8	17	2553	0.502093	0.000197	0.002193	341	0
	9	19	3695	0.537908	0.000146	0.001624	252	0
	10	21	4945	0.570380	0.000115	0.001286	200	0
	11	23	6403	0.602159	0.000094	0.001049	163	0
	12	25	8217	0.632993	0.000077	0.000859	133	0
	13	27	10395	0.662550	0.000064	0.000711	110	0
	14	29	12893	0.690378	0.000054	0.000597	92	0
	15	31	15515	0.714871	0.000046	0.000514	79	0
	16	33	18853	0.736313	0.000039	0.000436	67	0
	17	35	22575	0.756775	0.000034	0.000374	58	0
	18	37	26745	0.775988	0.000029	0.000324	50	0
	19	39	31103	0.795200	0.000026	0.000285	44	0
	20	41	36137	0.814413	0.000023	0.000251	39	0
	21	43	41851	0.833376	0.000020	0.000222	34	0
	22	45	47833	0.845364	0.000018	0.000197	30	0
	23	47	54435	0.857352	0.000016	0.000176	27	0
	24	49	61565	0.870450	0.000014	0.000158	24	0
	25	51	69599	0.884996	0.000013	0.000142	22	0
	30	61	119009	0.949487	0.000008	0.000089	13	0
	36	73	203965	0.959924	0.000005	0.000052	8	0
Silica fume	0	1	1	1.000000	1.000000	1.000000	160,264	160,264

3.3.2 Distribution of the cement phases

The single-phase microstructure image created in the preceding step is then turned into a four-phase image by distributing the proportions of C_3S, C_2S, C_3A and C_4AF. In this case, the number of moles of those compounds present in a 100 g of cement amount to $x = 0.209$, $y = 0.141$, $z = 0.048$ and $w = 0.016$, respectively. From this, the composition of cement clinker is calculated in terms of its major phases (Table 3-5).

Ideally, the three-dimensional microstructure image is filtered using two-point correlation functions measured on the actual two-dimensional SEM (Scanning Electron Microscopy) images of the cement used. This is not possible in this case, since no SEM images of Cement I 42.5 from the Cement Database of the NIST site are available. Instead, we assumed that similar results would be obtained by distributing the major anhydrous cement phases according to the two-dimensional pattern described by a cement clinker whose composition matched closely. Consequently, it was selected the Dyckerhoff cement since it shares a relative similar chemical composition.

The presence of coarse aggregate particles in concrete is modelled as a flat plate of finite thickness, which is usually satisfactory for most applications because their surfaces typically have very low curvature compared to cement particles /Bullard 2000/. One such flat thin (10 µm) particle was added into the microstructure and can be seen in Figure 3-1.

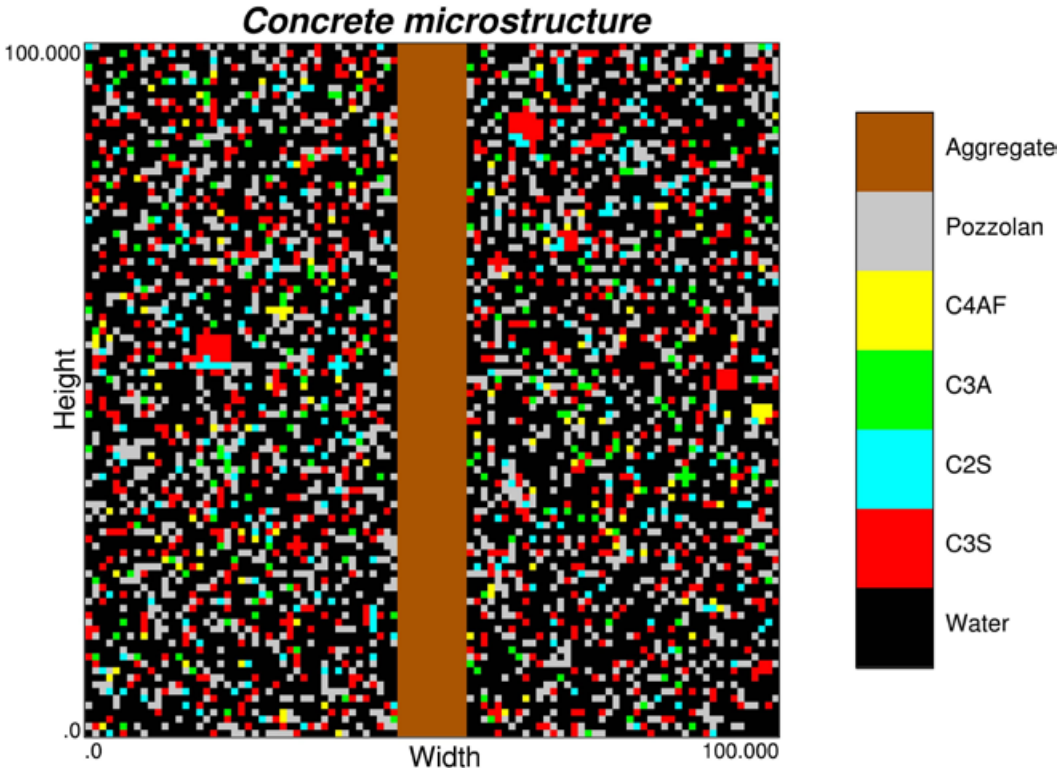

Figure 3-1. *Slice of the three-dimensional microstructure of the anhydrous cement mixture analyzed.*

Table 3-5. Mineralogical composition of the cement clinker for Cement I 42.5 MH/LA/SR.

Anhydrous compound	Volume percentage
C_3S	51.94
C_2S	25.90
C_3A	15.01
C_4AF	7.14

3.3.3 Simulation of hydration

Once the anhydrous mixture is sketched, the simulation of the hydration process is performed by means of another program included in the CEMHYD3D package, called Disreal3D. The simulation of hydration follows the hypothesis that the microstructural characteristics of the actual hydrated paste do not considerably differ from the simulated one, in spite of the different conditions of curing. The period of hydration considered for the simulation was of more than 100 days under saturated conditions and constant temperature of 25°C.

3.3.4 Results

The volume fractions of the components of the hydrated microstructure of concrete calculated by Disreal3D are shown in Table 3-6. The low volume fractions of anhydrous compounds confirm that hydration was almost complete. The hardened cement paste of concrete remains highly porous, in response to both the high water-to-cement ratio and the vicinity of the aggregate surface.

The addition of silica leads to the absence of portlandite and a high proportion of pozzolanic C-S-H, with lower calcium-to-silica ratio with respect to normal C-S-H. One two-dimensional slice of the generated microstructure of the hardened cement paste is shown in Figure 3-2.

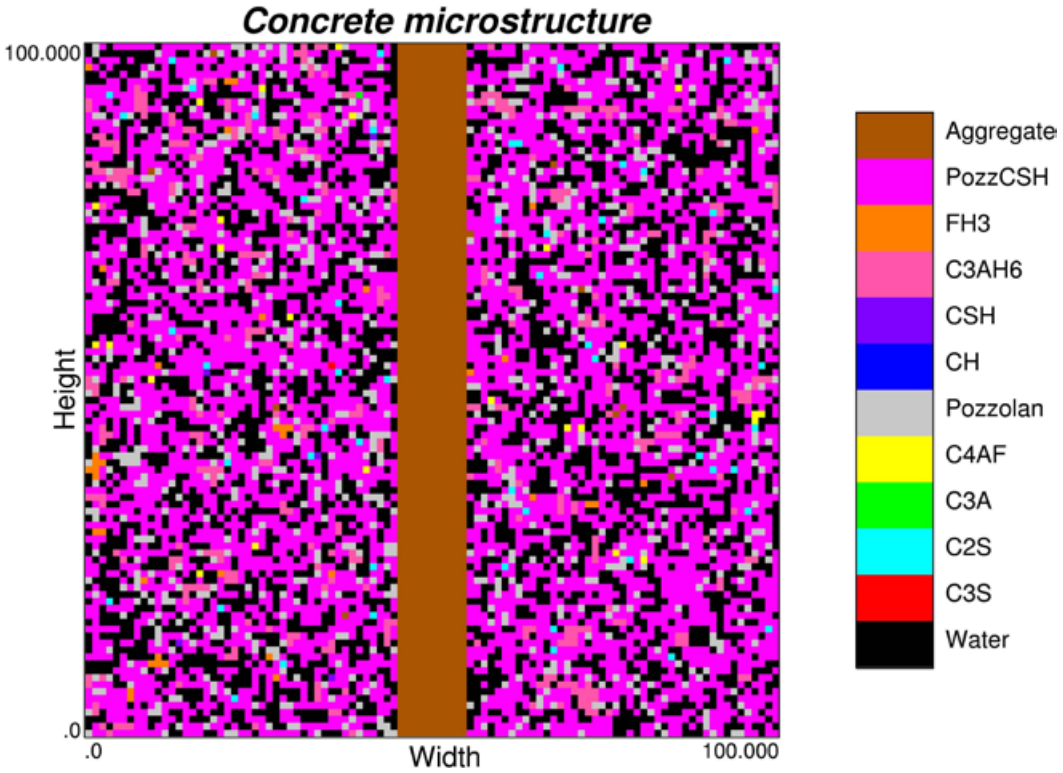

Figure 3-2. *Slice of the three-dimensional microstructure of the hydrated cement paste of the mix design analyzed.*

Table 3-6. Calculated volume fractions (%) for the mix design analyzed. CH = calcium hydroxide; C-S-H = calcium silicate hydrates ($C_{1.7}SH_4$); C_3AH_6 = katoite; FH_3 = iron hydroxide; PozzC-S-H = pozzolanic calcium silicate hydrates ($C_{1.1}SH_{3.9}$).

Component	Volume fraction (%)
Porosity	30.167
Silica fume	8.790
CH	0.013
C-S-H	0.045
C_3AH_6	4.425
FH_3	0.429
PozzC-S-H	45.208
Aggregate	10.000

4 Reactive transport models

4.1 Numerical code

Numerical simulations have been performed using the **CrunchFlow** code. The selection of this code is because the update of the transport properties and mineral reactive areas as a function of porosity changes is well tested and validated in a large number of examples in literature /e.g. Cochepin 2008/. **CrunchFlow** is a code written entirely in FORTRAN 90 and incorporates into a single code most of the features previously found in the GIMRT/OS3D package /Steefel and Yabusaki 1996, Steefel 2008/ along with a number of new features. The main features of the code include:

- Simulation of advective, dispersive, and diffusive transport in up to two dimension using the global implicit (GIMRT) option or three dimensions using time-splitting of transport and reaction (OS3D).
- Non-isothermal transport and reaction.
- Reaction-induced porosity and permeability feedback to both diffusion and flow.
- Unsaturated (gas-liquid) transport with equilibrium gas-aqueous phase exchange.
- Multicomponent diffusion with an electrochemical migration term to correct for electroneutrality where diffusion coefficients of charged species differ.

4.2 Initial and boundary conditions

4.2.1 Concrete composition and connected porosity

Hydration calculations show that concrete is initially made up with CSH with a Ca/Si ratio around 1.1, with a volume fraction of 45.21% (see Table 3-6). Other major compounds are silica fume (8.79%), katoite (C_3AH_6, 4.43%) and iron hydroxides (FH_3, 0.43%). Low-reactivity aggregate is predicted to be found at 10% in volume in the hydrated cement mixture. The remaining porosity is 30.17%; however, this value includes all pore sizes, most of them are unconnected. Consequently, the water-conductive porosity is expected to be much lower, being only restricted to larger pores. An example of the large pore size distribution in low-pH cements is recently reported by /Yamamoto et al. 2007/ (Figure 4-1).

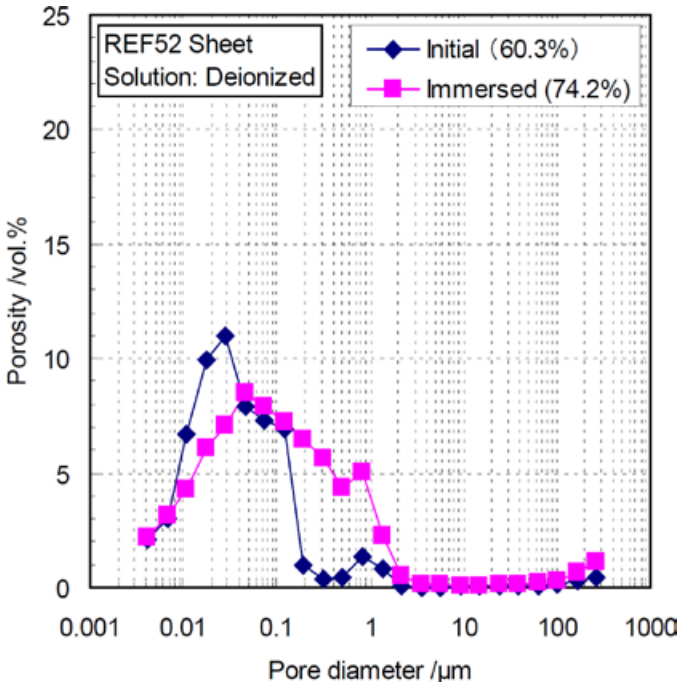

Figure 4-1. *Change of pore size distribution during the thin plate leaching tests from /Yamamoto et al. 2007/. The percentages in the legend refer to total porosity.*

In the model parameter calibration to reproduce the /Yamamoto et al. 2007/ experiments, /Grandia et al. 2010/ found that an initial connected porosity of 10% could account for the degradation profiles reported in these experiments. Consequently, as a initial condition, this value is considered in the numerical model for the alteration of the concrete in the present study.

The difference between the calculated porosity (30.17%) and the model porosity (10%) has been assumed to be a non-reactive aggregate. Similarly, the iron hydroxides have also been treated as a non-reactive mineral phases.

The initial Ca-Si ratio of CSH in the model is 1.13. The CSH compositions allowed to form (and to dissolve if become undersaturated) are the same as in Table 2-2. Also silica and katoite are initially present in the volume fractions above indicated. In addition, calcite, gypsum and ettringite, which are not initially present, can precipitate and dissolve. The formation of these secondary Ca-minerals is of great interest since (1) they can clog the porosity and (2) ettringite could cause mechanical breaking due to its large molar volume compared to the initial phases. In addition, the high Mg concentration in the backfill porewater could lead to Mg diffusion to concrete and cause saturation with dolomite; therefore, this mineral has also been included as a potential secondary phase.

All mineral phases are treated in a kinetic way. The precipitation-dissolution rate constant (k) for CSH is not precisely known but is believed to be quite close to the local equilibrium condition if the solute transport is driven by molecular diffusion. In this project, a values of $k = 1\times10^{-5}$ $mol_{CSH}\cdot m^{-3}_{rock}\cdot s^{-1}$, has been assumed. For other minerals the selected rates are as follows: katoite, 1×10^{-8} $mol_{Kat}\cdot m^{-3}_{rock}\cdot s^{-1}$, calcite, 3.2×10^{-7} $mol_{Cc}\cdot m^{-3}_{rock}\cdot s^{-1}$, ettringite, 1×10^{-8} $mol_{Et}\cdot m^{-3}_{rock}\cdot s^{-1}$, dolomite, 2.8×10^{-8} $mol_{Dol}\cdot m^{-3}_{rock}\cdot s^{-1}$, gypsum, 1×10^{-6} $mol_{Gy}\cdot m^{-3}_{rock}\cdot s^{-1}$.

The role of silica in low-pH concretes is to release Si to promote the formation of Si-rich CSH phases stable with relatively low-pH (less than 11). Consequently, the selection of a dissolution rate for silica appears to be an important parameter. In this project, silica is assumed to be of low reactivity and a rate constant of 1×10^{-9} $mol_{SiO2}\cdot m^{-3}_{rock}\cdot s^{-1}$ has been considered.

The modelling of concrete alteration has to deal with another fundamental uncertainty, which is the change in the molar volumes of the newly formed CSH phases. This change may have great importance in the porosity variations, especially if the reactive transport simulations include the coupling between porosity changes and hydraulic permeability, as done in the present study. In general, there is some rough, negative correlation between the molar volume of the crystalline CSH (e.g. tobermorite) with Ca-Si ratio (Table 4-1 and Figure 4-2). However, there is no evidence that gel-like CSH phases follow the same trend. On the other hand, the increase of molar volume as the alteration proceeds does not necessarily mean that porosity clogging is going to occur. If it is considered that CSH replacement is essentially a Ca-loss from the gel, and then the molar volumes are normalised to 1 mol of Si, the net volume of the gels decreases with the Ca-Si ratio (Figure 4-3).

Table 4-1. Molar volume of some crystalline CSH phases, which increases as the Ca/Si decreases. Normalised molar volumes respect to 1 mol of Si are also shown.

Mineral	Formula	Ca/Si ratio	Molar volume ($cm^3\cdot mol^{-1}$)	Molar Volume (normal vs. Si)	Ref.
Reinhardbraunsite	$Ca_5(SiO_4)2(OH,F)_2$	2.50	145.79	72.89	(1)
Dellaite	$Ca_6Si_3O_{11}(OH)_2$	2.00	181.46	60.48	(1)
Bultfonteinite	$Ca_2SiO_2(OH,F)_4$	2.00	76.63	76.63	(1)
Hillebrandite	$Ca_2SiO_3(OH)_2\cdot0.17(H_2O)$	2.00	71.79	71.79	(2)
Afwillite	$Ca_3Si_2O_4(OH)_6$	1.50	130.71	65.35	(3)
Jennite	$Ca_9Si_6O_{18}(OH)_6\cdot8H_2O$	1.50	458.35	76.39	(3)
Foshagite	$Ca_4Si_3O_9(OH)_2\cdot0.5(H_2O)$	1.33	124.23	41.41	(2)
Xonotlite	$Ca_6Si_6O_{17}(OH)_2$	1.00	264.81	44.14	(2)
Tobermorite	$Ca_5Si_6O_{16}(OH)_2\cdot4(H_2O)$	0.83	300.81	50.13	(3)
Gyrolite	$Ca_2Si_3O_7(OH)_2\cdot1.5(H_2O)$	0.83	136.85	45.62	(4)
Okenite	$CaSi_2O_4(OH)_2\cdot(H_2O)$	0.50	94.77	47.38	(2)

(1) /Institute of Experimental Mineralogy 1997/, (2) /Jennings 1986/, (3) /Bourbon 2003 cited in Gaucher et al. 2004/, (4) /Clodic and Meike 1997/.

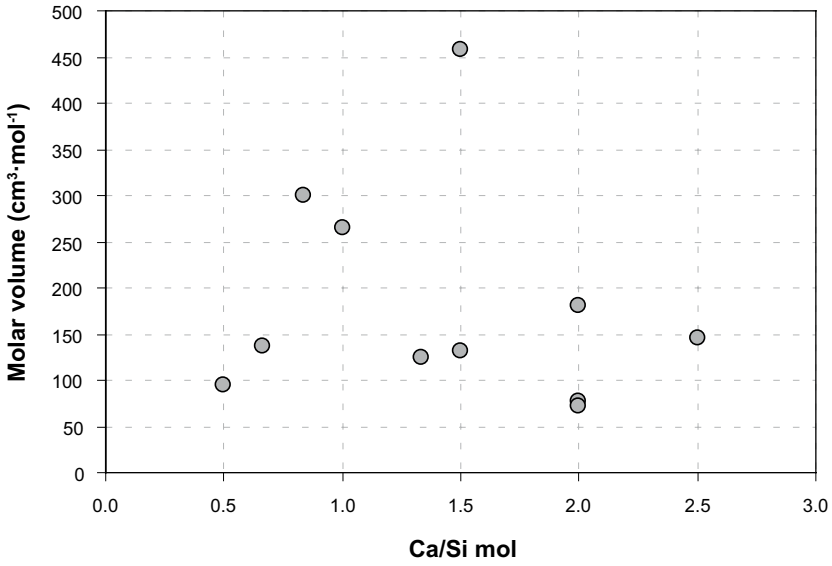

Figure 4-2. *Molar volumes of crystalline CSH phases as a function of their Ca-Si ratio (see Table 4-1 for references).*

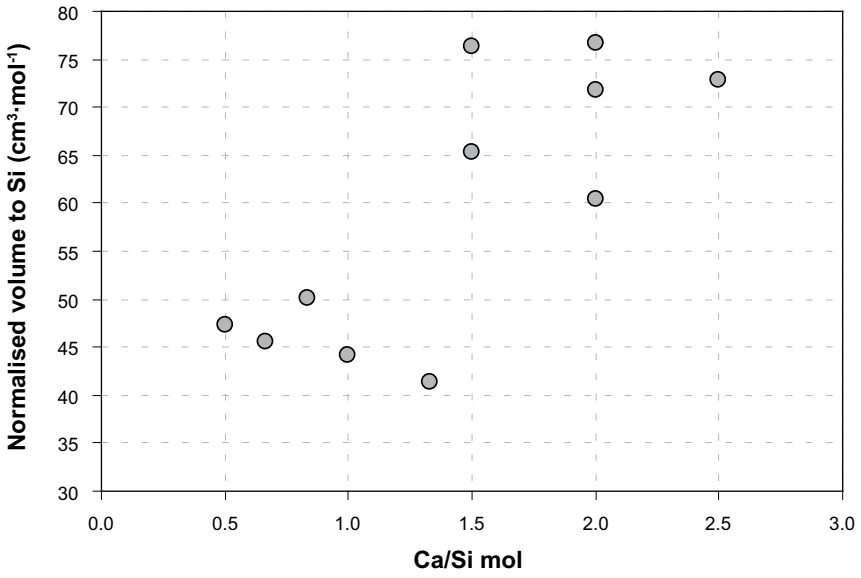

Figure 4-3. *Molar volumes of crystalline CSH phases – normalised to 1 mol of Si – as a function of their Ca-Si ratio (see Table 4-1 for references).*

As a reasonable approach considering the existing data, an intermediate value between the crystalline CSH with Ca/Si=2 and the CSH with Ca/Si=0.83 has been considered for all CSH phases (160 $cm^3 \cdot mol^{-1}$).

A similar uncertainty is found for ettringite, which have a very large molar volume. In the model, a value of 500 $cm^3 \cdot mol^{-1}$ is assumed.

For other minerals, the molar volumes considered are shown in Table 4-2.

Table 4-2. Molar volumes for calcite, dolomite, gypsum, silica and katoite.

Mineral	Molar volume ($cm^3 \cdot mol^{-1}$)
Calcite	36.93
Dolomite	64.34
Gypsum	74.69
Silica	29.00
Katoite	149.52

4.2.2 Backfill composition and related porosity

The backfill considered in this project is assumed to consist basically (69 wt%) of Milos-type bentonite. The mineralogical and physical properties are described in /Olsson and Karnland 2009/. Accessory mineral concentration is shown in Table 4-3, and includes dolomite, quartz, calcite and gypsum. Small amounts of pyrite are also reported; however, iron system is not considered in the model and, therefore, this mineral is assumed to be a non-reactive phase. The dissolution-precipitation kinetics is the same as indicated in Section 4.2.1.

The geochemistry of the backfill porewater is not only controlled by the accessory minerals but also by the ionic exchange capacity in the clay fraction. The buffer effect of the exchange sites may influence the geochemical gradients between backfill and concrete, including pH. In the simulations performed in the project, surface exchange in the backfill is not considered in order to assume a conservative condition to evaluate the penetration capacity of alkaline fluids from concrete to backfill.

Finally, hydraulically-connected porosity is 44%, following /Åkesson et al. 2010/.

4.2.3 Initial and boundary waters

Three water types are initially present in the system: (1) concrete pore water, (2) backfill pore water, and (3) granitic, Forsmark-type water.

The initial composition of the pore water in equilibrium with concrete is rather difficult to determine applying thermodynamics. Low-pH concrete consists of CSH and silica fume mixtures. The solid solution approach of /Sugiyama and Fugita 2006/ considers that CSH's are intermediate solids between $Ca(OH)_2$ and $SiO_{2(am)}$; therefore it is clear that any solution can not met equilibrium with CSH and $SiO_{2(am)}$ at the same time. Since CSH is volumetrically more important in the concrete and shows a faster kinetics, the initial composition of pore water in the model is considered to be in equilibrium with CSH of Ca/Si= 1.13–1.17 (Table 4-4). The other CSH phases and end members of the solid solution are undersaturated (Table 4-5). In addition, potential secondary minerals are also undersaturated. An additional unknown in the model is the aluminium concentration in the concrete porewater. To keep consistency in the initial equilibrium, the aluminium concentration has been calculated forcing the thermodynamic equilibrium with katoite, which is already present in the concrete mixture. The resulting value is 1.45×10^{-5} $mol \cdot L^{-1}$. All the calculations have been done considering the aqueous species listed in Table 4-6.

The equilibrium with CSH of Ca/Si ~ 1.1 leads to an initial pH of 12.0.

Table 4-3. Volume fraction of accessory minerals.

Mineral	Volume fraction (%)
Calcite	3.11
Dolomite	5.92
Gypsum	0.36
Silica	0.28

Table 4-4. Chemistry of concrete pore water, backfill pore water and granitic groundwater (solutes in mol·L^{-1}).

	Granitic water	Concrete pore water	Backfill pore water
T(ºC)	25	25	25
pH	7.2	12.0	7.14
SiO_2(aq)	1.85×10^{-4}	3.58×10^{-6}	1.69×10^{-4}
Na	8.88×10^{-2}	7.14×10^{-2}	2.92×10^{-2}
K	8.75×10^{-4}	1.09×10^{-1}	2.38×10^{-1}
Ca	2.33×10^{-2}	6.50×10^{-2}	3.00×10^{-2}
C(IV)	2.20×10^{-3}	9.00×10^{-6}	1.12×10^{-3}
Sulphate	6.80×10^{-3}	5.00×10^{-5}	1.50×10^{-2}
Cl	1.53×10^{-1}	1.46×10^{-3}	1.38×10^{-1}
Mg	9.30×10^{-3}	1.00×10^{-4}	1.30×10^{-2}
Al	1.00×10^{-8}	1.46×10^{-5}	1.00×10^{-8}

Table 4-5. Saturation index – log (IAP/K) – of mineral phases considered in the simulations with respect to concrete pore water, backfill pore water and granitic groundwater. The figure following CSH indicates the Ca-Si ratio.

Mineral	Granitic Gw	Concrete pore water	Backfill pore water
CSH_1.33	–9.69	–0.03	–9.15
CSH_1.27	–9.10	–0.02	–8.60
CSH_1.22	–8.56	–0.01	–8.07
CSH_1.17	–8.04	0.00	–7.57
CSH_1.13	–7.55	0.00	–7.10
CSH_1.08	–7.09	–0.01	–6.66
CSH_1.04	–6.65	–0.03	–6.24
CSH_1.00	–6.25	–0.06	–5.85
CSH_0.96	–5.87	–0.09	–5.49
CSH_0.92	–5.52	–0.14	–5.15
CSH_0.89	–5.19	–0.20	–4.84
CSH_0.85	–4.88	–0.26	–4.55
CSH_0.82	–4.47	–0.21	–4.15
CSH_0.79	–4.24	–0.33	–3.94
CSH_0.75	–4.05	–0.46	–3.76
CSH_0.72	–3.88	–0.62	–3.60
CSH_0.69	–3.74	–0.79	–3.47
CSH_0.67	–3.76	–1.11	–3.51
CSH_0.64	–3.51	–1.15	–3.27
CSH_0.61	–3.42	–1.34	–3.19
CSH_0.56	–3.26	–1.72	–3.06
CSH_0.52	–3.13	–2.09	–2.94
SiO_2(am)	–1.01	–5.45	–1.04
Calcite	0.00	–0.08	0.00
Dolomite	0.00	–2.65	–0.04
Katoite	–28.09	0.00	–27.06
Gypsum	–0.58	–2.41	–0.08
Ettringite	–26.85	–4.24	–24.32

Table 4-6. Aqueous species considered in the calculations.

Element	Aqueous species
H	H^+ , OH^-
Al	Al^{3+}, $Al(OH)_2^+$, $AlSO_4^+$, $Al(SO_4)_2^-$, $Al(OH)^{3-}$
Ca	Ca^{2+} , $Ca(OH)^+$, $CaCO_{3\,(aq)}$, $CaHCO_3^+$, $CaSO_{4\,(aq)}$
Si	$SiO_{2\,(aq)}$, $HSiO_3^-$, $H_2SiO_4^{2-}$, $H_4(H_2SiO_4)_4^{4-}$, $H_6(H_2SiO_4)_4^{2-}$
Na	Na^+, $NaCO_3^-$,$NaOH_{(aq)}$, $NaCO_3^-$, $NaHCO_{3\,(aq)}$, $NaHSiO_{3\,(aq)}$, $NaSO_4^-$
K	K^+ , $KOH_{(aq)}$, $KHSO_{4\,(aq)}$, KSO_4^-
Mg	Mg^{2+}, $Mg(OH)^+$, $MgCO_{3\,(aq)}$, $MgHCO_3^+$, $MgCl^+$
Cl	Cl^-
S(VI)	SO_4^{2-} , HSO_4^-, $H_2SO_{4\,(aq)}$
C(IV)	CO_3^{2-}, HCO_3^-, CO_3^{2-}

The backfill pore water is calculated from the geochemical equilibrium between granitic water (Formark composition) and backfill (with Milos-type bentonite) (Table 4-4). At this point it is worth mentioning that the total length of backfill in the modelled domain is only 0.3 m, which is much shorter than in the reality. The consideration of smaller amounts of backfill is for calculation simplicity and because the project interest is found in the backfill-concrete boundary, not deep inside the backfill. The effect of a larger pore water volume is represented in the model as a fixed chemistry in the boundary condition.

Finally, a typical deep groundwater at Forsmark has been selected as external groundwater. This is a neutral, saline (essentially Na and Cl) water. Also, it contains moderate concentrations of calcium, sulphate and carbonate (Table 4-4). It is significantly undersaturated with respect to CSH gels.

The temperature for water-concrete reaction is in all cases set to 25ºC.

4.2.4 Solute transport and flow boundary conditions

As already mentioned in the definition of the model domain, advective solute flow is limited to the fracture. In the numerical model, this is represented considering a fixed solute composition in the element corresponding to fracture. As a consequence, a quick renewal of granitic groundwater is ensured, leading to a chemically "aggressive" boundary condition. Inside the concrete and through the backfill, solutes move due to concentration gradients, i.e. by molecular diffusion. The coefficient of molecular diffusion has been set to 5×10^{-10} $m^2\cdot s^{-1}$.

4.2.5 Simulation time

The reactive transport simulation has been run for 1,000 years. Preliminary simulations at longer times revealed that the progressive decrease of porosity in the concrete slows down the solute transport and the interaction between external water and the concrete is extremely small at times higher than 1,000 years.

4.3 Results

The predicted effects of the geochemical interaction between fluids in granite, concrete and backfill after one year are restricted to the material contacts. The most relevant process, although transitory, is the alkaline pH intrusion (pH>11) up to 6 cm into the backfill (Figure 4-4). In contrast, alkaline pH does not affect granitic groundwater, mainly caused by the forced water renewal in the fracture. Mineralogical changes are predicted in both concrete and backfill (Figure 4-5 and Figure 4-6):

1) CSH replacement from Ca-richer phases ($C_{1.13}SH$) to Si-richer phases ($C_{1.04}SH$, $C_{1.00}SH$, $C_{0.82}SH$), and ettringite formation, and
2) carbonate precipitation in the fracture and in the backfill. As a consequence of these mineralogical changes, porosity decreases slightly (between 1.5 and 3%).

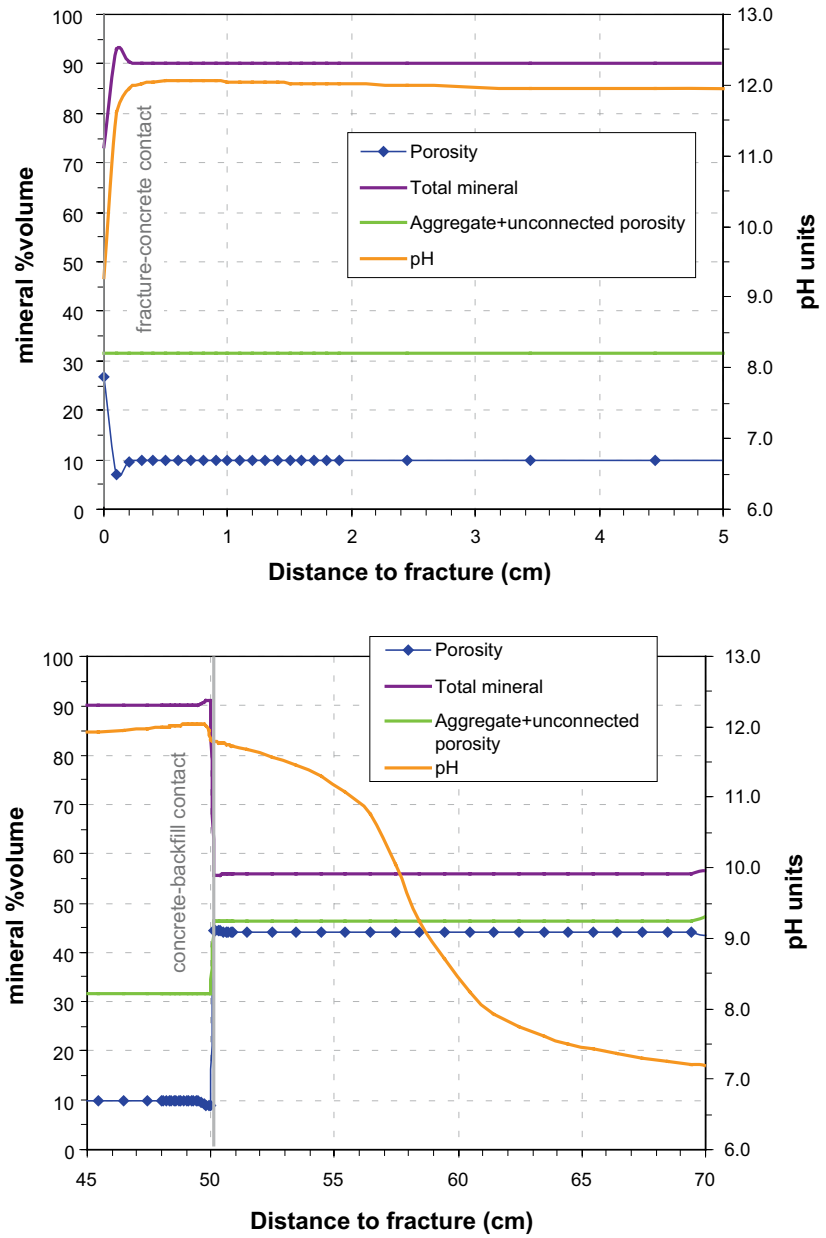

Figure 4-4. *Predicted composition of pore water, porosity and pH in concrete and backfill after 1 year of simulation in fracture-concrete and concrete-backfill contacts. Unconnected porosity and non-reactive aggregate in the concrete and backfill are plot together.*

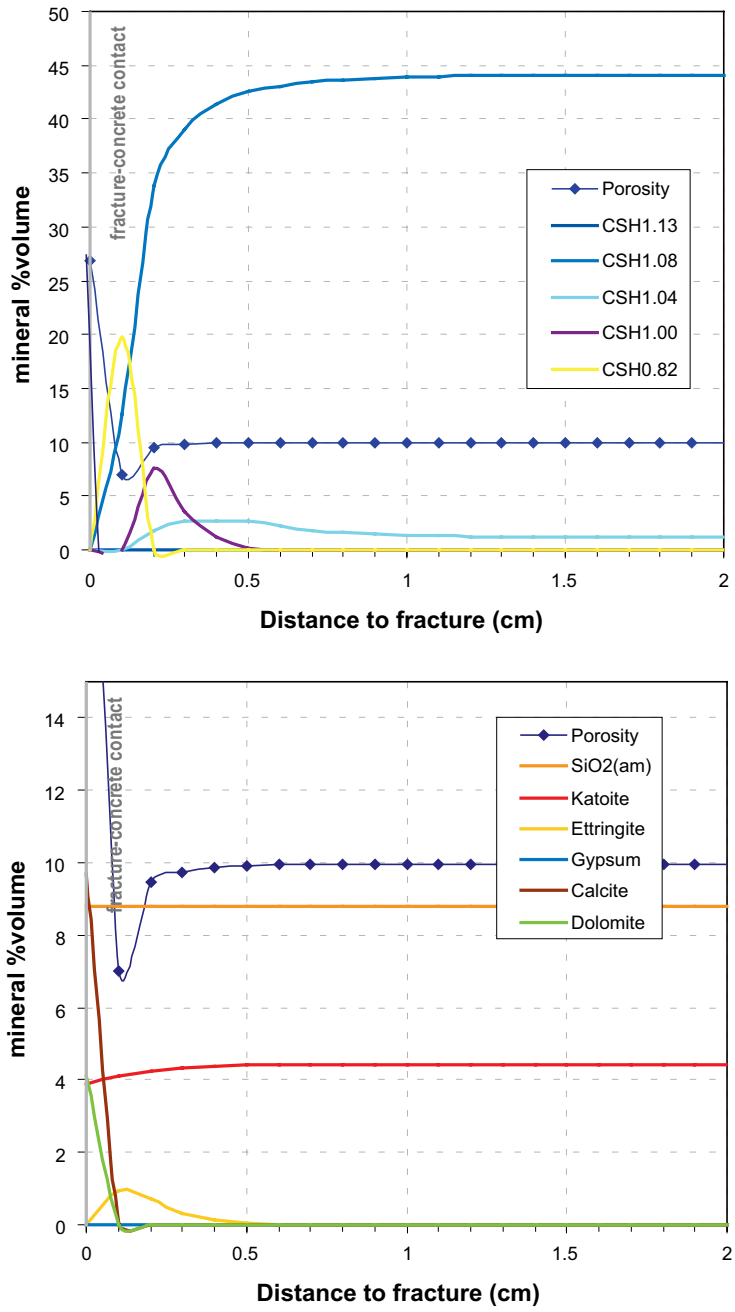

Figure 4-5. *Predicted composition of calcium-silicate-hydrates (CSH) and accessory minerals in the fracture-concrete contact after 1 year. Figures of CSH in the legend indicate the Ca-Si ratio.*

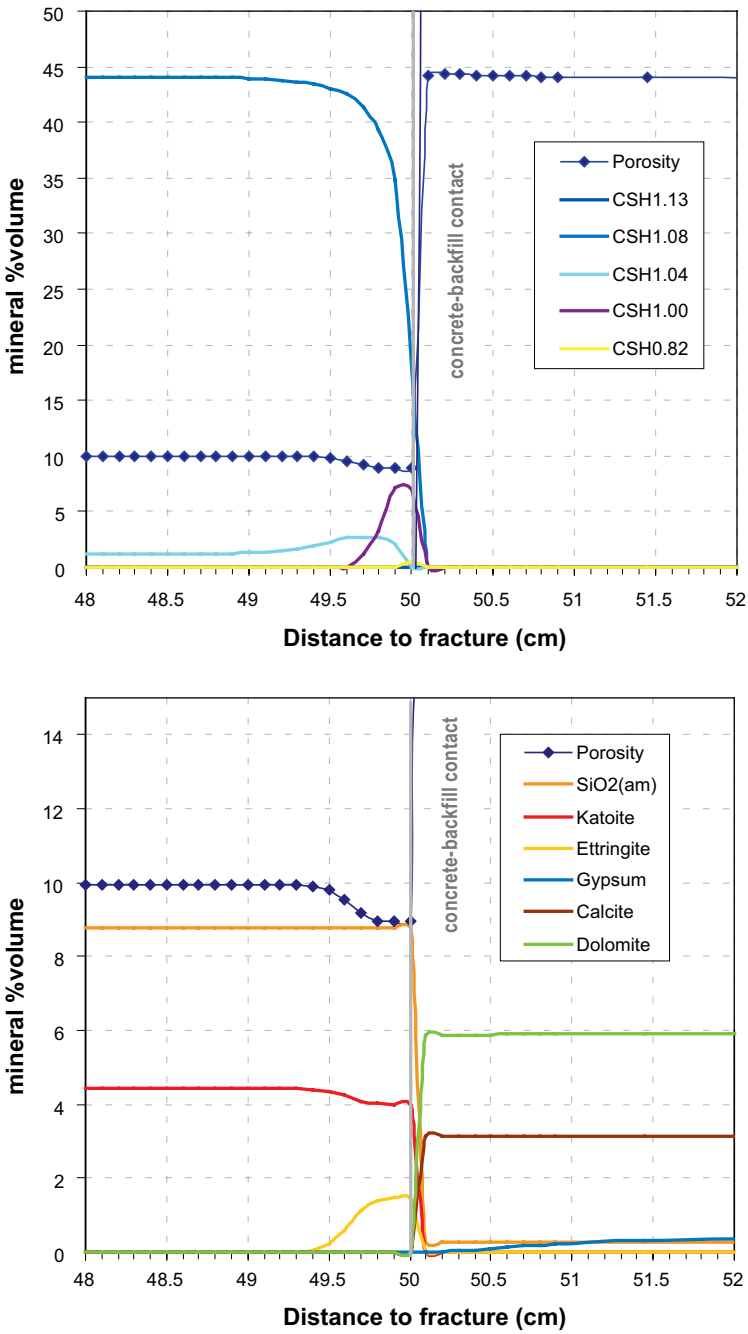

Figure 4-6. *Predicted composition of calcium-silicate-hydrates (CSH) and accessory minerals in the concrete-backfill contact after 1 year. Figures of CSH in the legend indicate the Ca-Si ratio.*

At longer times (10 years), porosity begins to clog due to CSH replacement and ettringite formation, especially in the granite-concrete boundary (Figure 4-7 and Figure 4-8). At the backfill-concrete contact, alkaline-pH plume vanishes and ettringite precipitation reaches up 10 vol.% forced by katoite dissolution (Figure 4-9).

The model predicts insignificant modifications in the geochemistry of the system from 10 to longer times since porosity has already been clogged at both concrete boundaries (Figure 4-10, Figure 4-11 and Figure 4-12), decreasing the diffusion between material pores. CSH phases keep replacing from Ca-rich to Si-rich intermediates.

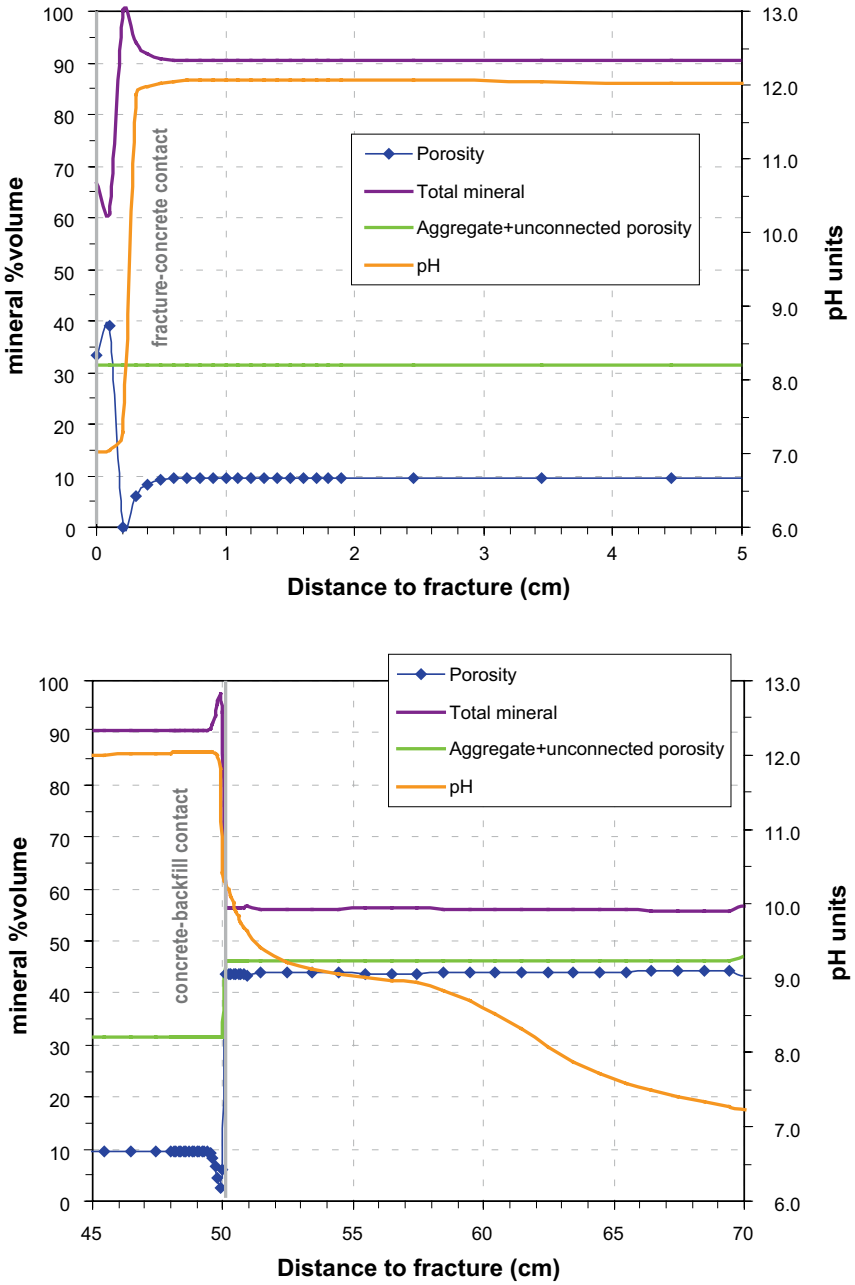

Figure 4-7. *Predicted composition of pore water, porosity and pH in concrete and backfill after 10 years of simulation in fracture-concrete and concrete-backfill contacts. Unconnected porosity and non-reactive aggregate in the concrete and backfill are plot together.*

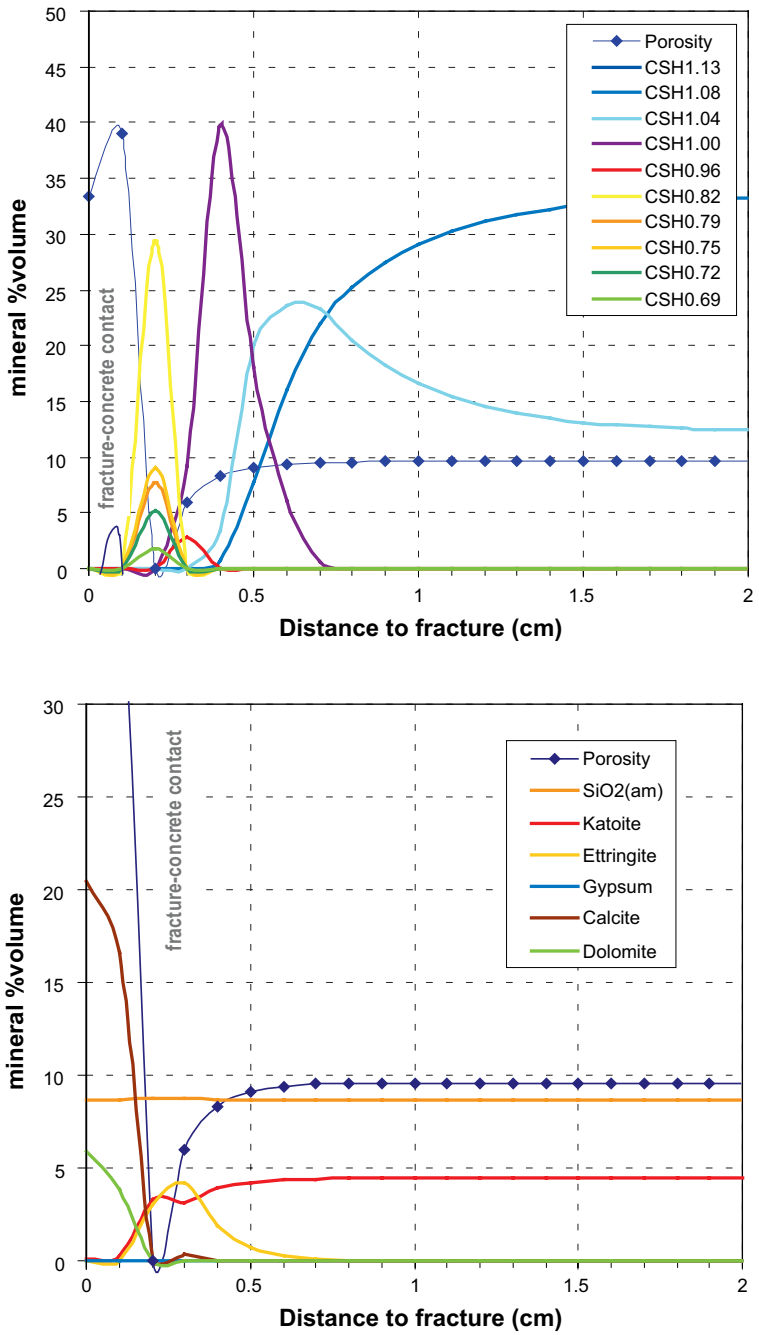

Figure 4-8. *Predicted composition of calcium-silicate-hydrates (CSH) and accessory minerals in the fracture-concrete contact after 10 years. Figures of CSH in the legend indicate the Ca-Si ratio.*

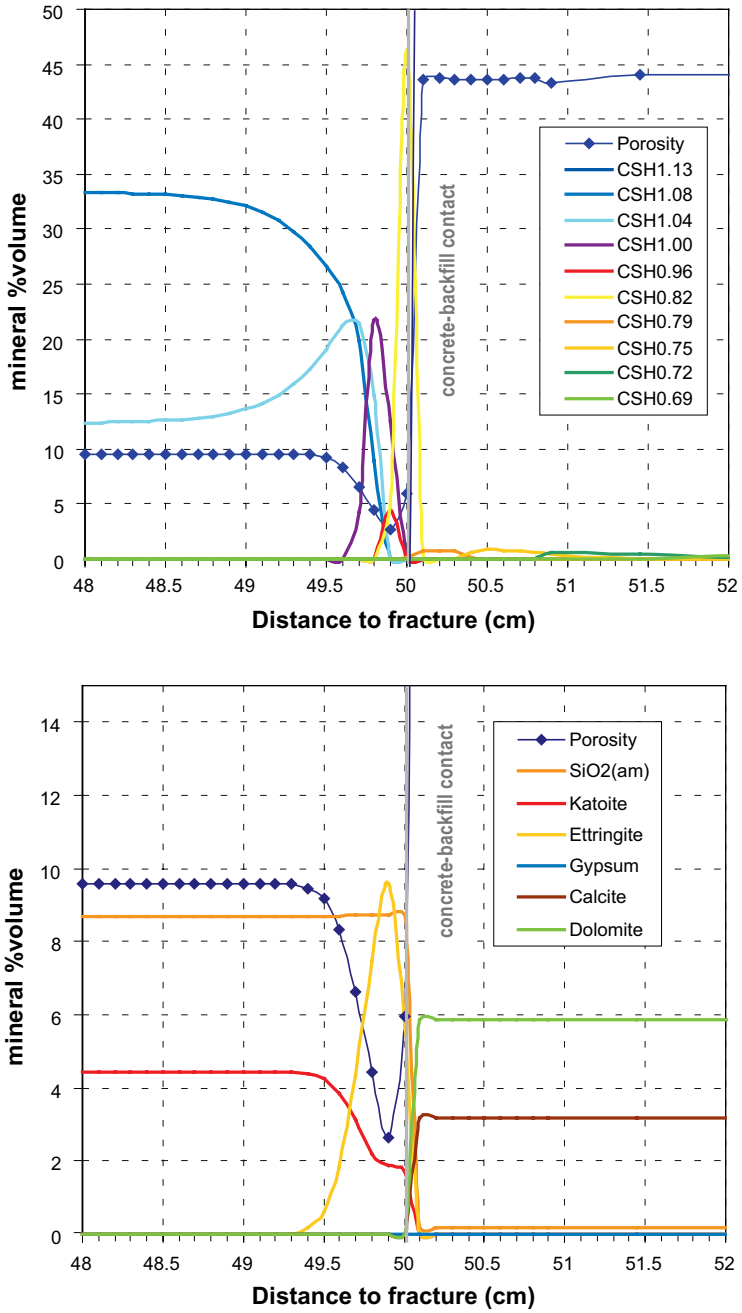

Figure 4-9. *Predicted composition of calcium-silicate-hydrates (CSH) and accessory minerals in the concrete-backfill contact after 10 years. Figures of CSH in the legend indicate the Ca-Si ratio.*

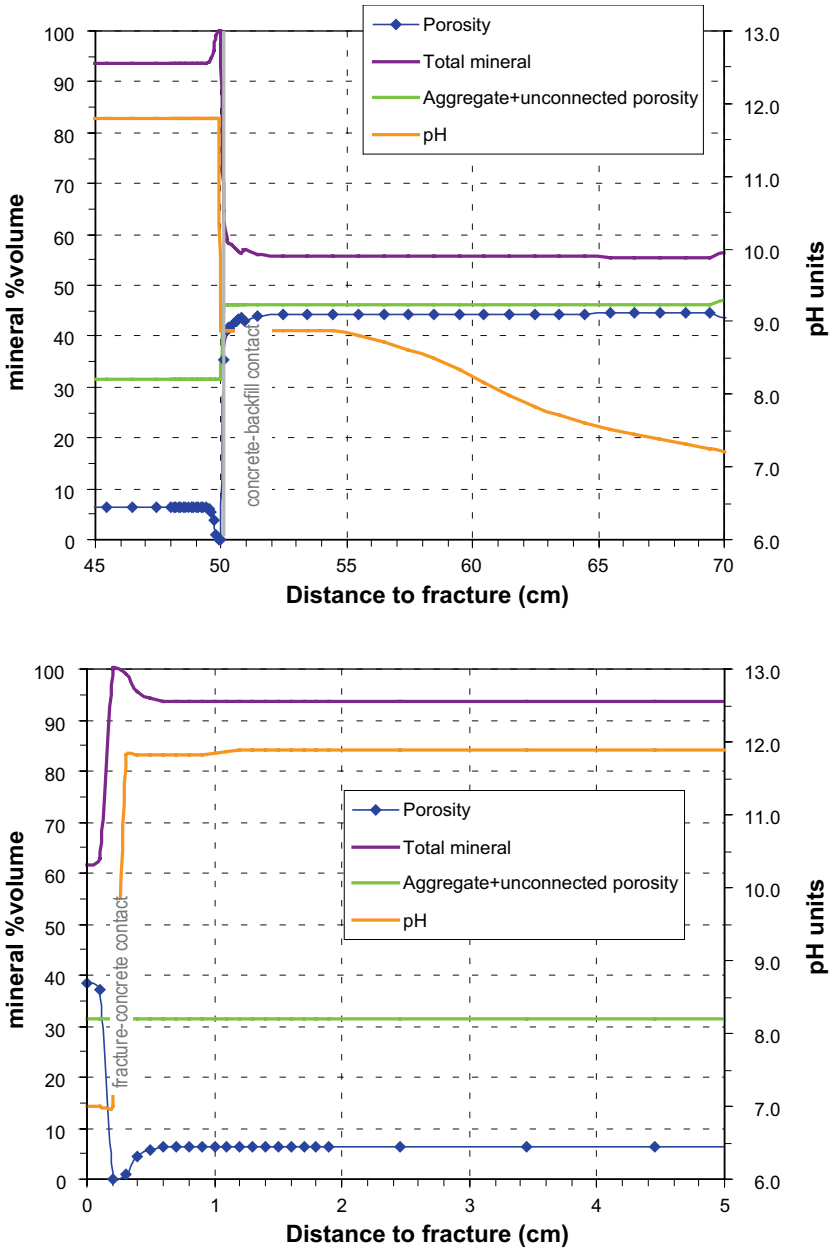

Figure 4-10. *Predicted composition of pore water, porosity and pH in concrete and backfill after 100 years of simulation in fracture-concrete and concrete-backfill contacts. Unconnected porosity and non-reactive aggregate in the concrete and backfill are plot together.*

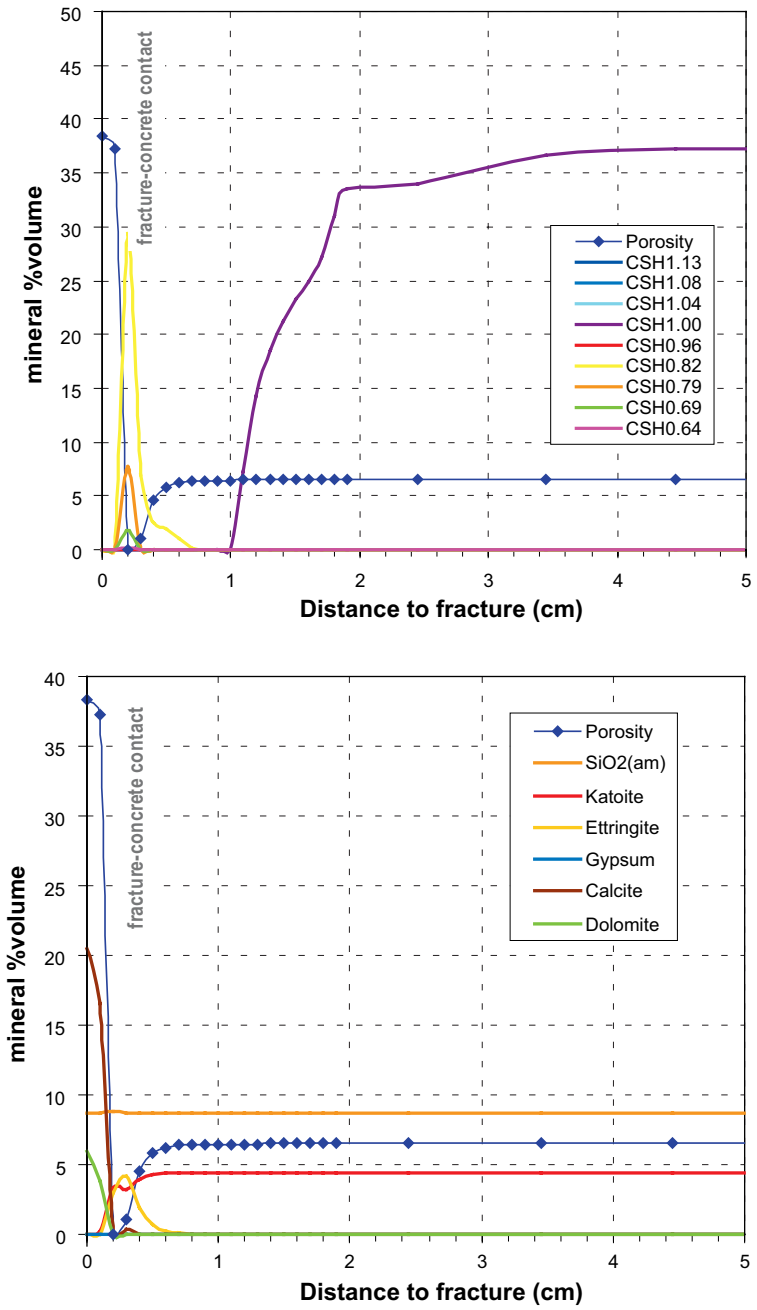

Figure 4-11. *Predicted composition of calcium-silicate-hydrates (CSH) and accessory minerals in the fracture-concrete contact after 100 years. Figures of CSH in the legend indicate the Ca-Si ratio.*

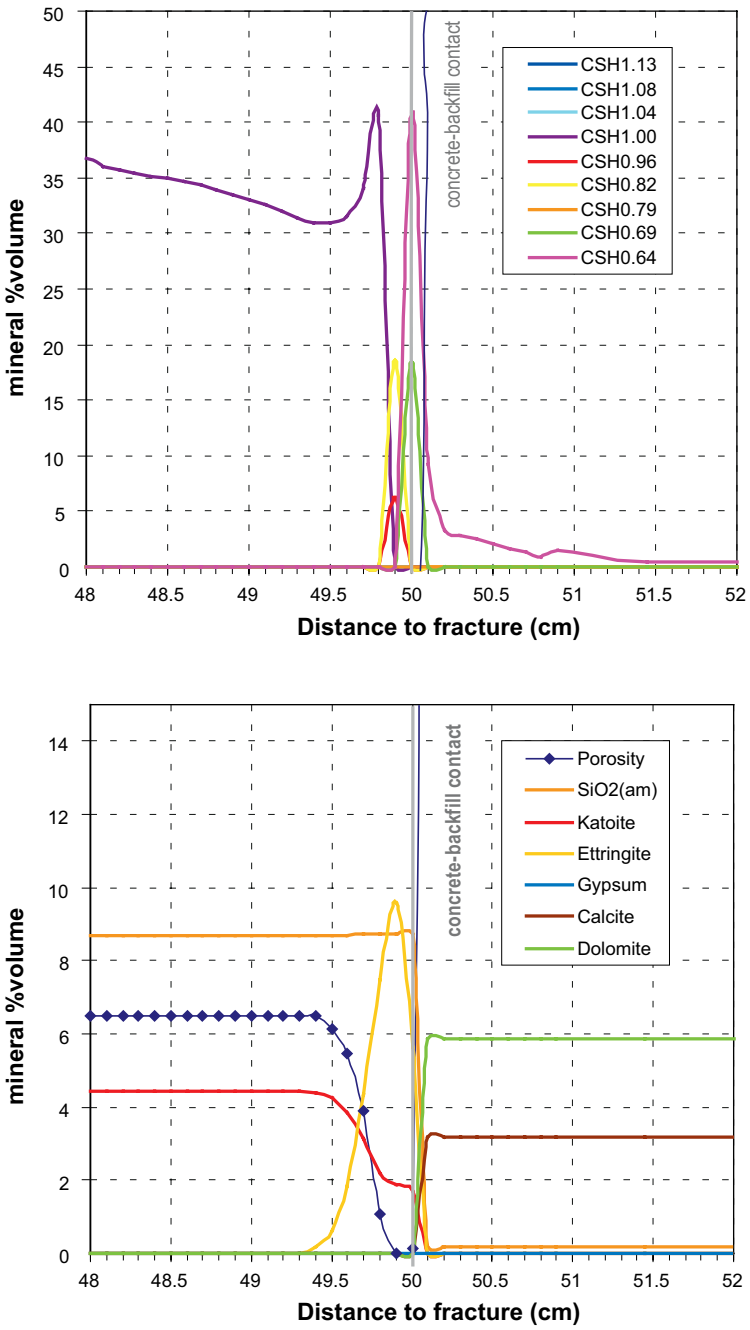

Figure 4-12. *Predicted composition of calcium-silicate-hydrates (CSH) and accessory minerals in the concrete-backfill contact after 100 years. Figures of CSH in the legend indicate the Ca-Si ratio.*

5 General discussion and conclusions

The results from reactive transport simulations predict that the effect of low-pH concrete alteration on the stability of backfill materials is low. Dissolution of CSH phases causes a initial hyperalkaline plume (pH>11) penetrating ~6 cm into the backfill. This plume is transient since in a few years (<10 y), pH decreases back to more circumneutral values. The main process governing geochemistry in the backfill-concrete boundary is the quick loss of porosity due to ettringite precipitation. The very high molar volume (500 $cm^3 \cdot mol^{-1}$) of this mineral enhances the rate of clogging. The ettringite formation is mainly driven by the high sulphate concentration in the backfill porewater (1.50×10^{-2} $mol \cdot L^{-1}$), which in turn is controlled by the equilibrium with gypsum. The release and diffusion of calcium (from CSH replacement) and Al (from katoite dissolution) from concrete causes ettringite precipitation at the concrete-backfill boundary.

The loss of porosity dramatically reduces solute diffusion and, consequently, the backfill-concrete system remains almost invariably for the next hundreds of years. Only CSH replacement occurs following a kinetically-driven decalcification.

On the other hand, the potential transfer of solutes from the granitic water is negligible since concrete quickly buffers the system. Initial CSH is replaced by low Ca phases (Ca/Si= 1.00 to 0.82). In addition, the coeval formation of ettringite formation leads to a porosity clogging between 10 and 100 years. As in the backfill-concrete case, the evolution of the fracture-concrete system is almost invariable at times longer than 100 years.

The role of ettringite precipitation must be evaluated in detail since porosity clogging may force mechanical instabilities in the concrete, which would cause significant geochemical and hydraulic consequences. The initial concentrations of Al considered in this work are not obtained from pore water analysis but based on thermodynamic assumptions. To build a more accurate prediction, it is needed a determination of Al concentration in concrete and backfill pore waters in detail.

Additional uncertainties that can affect the final model results are the CSH molar volumes, the solute diffusion coefficients and the rates of mineral dissolution-precipitation.

To summarize, the model predictions indicate that the durability of backfill materials is not expected to be affected by the potential alkaline plumes developed from concrete alteration. Unless secondary porosity occurred due to cracking, the loss of porosity prevents the formation of alkaline plumes and subsequent dissolution of backfill material.

6 References

SKB's (Svensk Kärnbränslehantering AB) publications can be found at www.skb.se/publications.

Arcos D, Domènech C, Grandia F, 2006. Geochemical evolution of the near field of a KBS-3 repository. SKB TR-06-16, Svensk Kärnbränslehantering AB.

Bentz D P, 1997. Three-dimensional computer simulation of portland cement hydration and microstructure development. Journal of the American Ceramic Society, 80, pp 3–21.

Bentz D P, 2000. CEMHYD3D: a three-dimensional cement hydration and microstructure development modelling package. Version 2.0, NISTIR 6485, U.S. Department of Commerce.

Bentz D P, Conway J T, 2001. Computer modeling of the replacement of "coarse" cement particles by inert fillers in low w/c ratio concretes: hydration and strength. Cement and Concrete Research, 31, pp 503–506.

Bentz D P, Coveney P V, Garboczi E J, Kleyn M F, Stutzman P E, 1994. Cellular automaton simulations of cement hydration and microstructure development. Modelling and Simulation in Materials Science and Engineering, 2, pp 783–808.

Bentz D P, Garboczi E J, Haecker C J, Jensen O M, 1999. Effects of cement particle size distribution on performance properties of Portland cement-based materials. Cement and Concrete Research, 29, pp 1663–1671.

Bentz D P, Haecker C J, 1999. An argument for using coarse cements in high-performance concretes. Cement and Concrete Research, 29, pp 615–618.

Bentz D P, Jensen O M, Hansen K K, Olesen J F, Stang H, Haecker C-J, 2000. Influence of cement particle-size distribution on early age autogenous strains and stresses in cement-based materials. Journal of the American Ceramic Society, 84, pp 129–135.

Berner U R, 1988. Modelling the incongruent dissolution of hydrated cement minerals. Radiochimica Acta, 44/45, pp 387–393.

Berner U R, 1992. Evolution of pore water chemistry during degradation of cement in a radioactive waste repository environment. Waste Management, 12, pp 201–219.

Bullard J W, 2000. User's guide to the virtual cement and concrete testing laboratory. Version 1.1. [Online]. Available at: http://purl.access.gpo.gov/GPO/LPS90605.

Börjesson S, Emrén A, Ekberg C, 1997. A thermodynamic model for the calcium silicate hydrate gel, modelled as a non-ideal binary solid solution. Cement and Concrete Research, 27, pp 1649–1657.

Carey J W, Lichtner P C, 2007. Calcium silicate hydrate (C-S-H) solid solution model applied to cement degradation using the continuum reactive transport model FLOTRAN. In: Mobasher B, Skalny J (eds). Transport properties and concrete quality: materials science of concrete, special volume. Hoboken, N.J.: Wiley, pp 73–106.

Chen J J, Thomas J J, Taylor H F W, Jennings H M, 2004. Solubility and structure of calcium silicate hydrate. Cement and Concrete Research, 34, pp 1499–1519.

Clodic L, Meike A, 1997. Thermodynamics of calcium silicate hydrates. Development of a database to model concrete dissolution at 25ºC using the EQ3/6 geochemical modelling code. UCRL-ID-132088, Lawrence Livermore National Laboratory.

Cochepin B, 2008. Approaches to modeling coupled flow and reaction in a 2-D cementation experiment. LBNL-809E, Lawrence Berkeley National Laboratory.

Dershowitz W, Winberg A, Hermansson J, Byegård J, Tullborg E-L, Andersson P, Mazurek M, 2003. Äspö Hard Rock Laboratory. Äspö Task Force on modelling of groundwater flow and transport of solutes. Task 6C. A semi-synthetic model of block scale conductive structures at the Äspö HRL. SKB IPR-03-13, Svensk Kärnbränslehantering AB.

du Plessis H, Kearsley E P, Matjie H, 2007. Effect of grinding time on the particle size distribution of gasification ash and Portland cement clinker. Journal of the South African Institution of Civil Engineering, 49, pp 28–34.

Flint E P, Wells L S, 1934. Study of the system CaO–SiO_2–H_2O at 30ºC and of the reaction of water on the anhydrous calcium silicates. Journal of research of the National Bureau of Standards, 12, pp 751–783.

Follin S, Stigsson M, Svensson U, 2005. Regional hydrogeological simulations for Forsmark – numerical modelling using DarcyTools. Preliminary site description Forsmark area – version 1.2. SKB R-05-60, Svensk Kärnbränslehantering AB.

Fujii K, Kondo W, 1981. Heterogeneous equilibria of calcium silicate hydrate in water at 30°C. Journal of the Chemical Society Dalton Transactions, 2, pp 645–651.

Galíndez J-M, Molinero J, Samper J, Yang C B, 2006. Simulating of concrete degradation processes by reactive transport models. Journal de Physique IV, 136, pp 177–188.

Gaucher E C, Blanc P, Matray J-M, Michau N, 2004. Modeling diffusion of an alkaline plume in a clay barrier. Applied Geochemistry, 19, pp 1505–1515.

Grandia F, Galíndez, J-M, Molinero J, Arcos D, 2010. Quantitative modelling of the degradation processes of cement grout. Project CEMMOD. SKB TR-10-25, Svensk Kärnbränslehantering AB.

Greenberg S A, Chang T N, 1965. Investigation of the colloidal hydrated calcium silicates. II. Solubility relationships in the calcium oxide–silica–water system at 25ºC. Journal of Physical Chemistry, 69, pp 182–188.

Harris A W, Manning M C, Tearle W M, Tweed C J, 2002. Testing of models of the dissolution of cements – leaching of synthetic CSH gels. Cement and Concrete Research, 32, pp 731–746.

Hartley L, Hoch A, Jackson P, Joyce S, McCarthy R, Rodwell W, Swift B, Marsic N, 2006. Groundwater flow and transport modelling during the temperate period for the SR-Can assessment. Forsmark area – version 1.2. SKB R-06-98, Svensk Kärnbränslehantering AB.

Institute of Experimental Mineralogy, 1997. Mincryst: crystallographic database for minerals. [Online]. Available at: http://database.iem.ac.ru/mincryst/.

Jennings H M, 1986. Aqueous solubility relationships for two types of calcium silicate hydrate. Journal of the American Ceramic Society, 69, pp 614–618.

Kalousek G, 1952. Application of differential thermal analysis in a study of the system lime–silica–water. In: Proceedings of the Third International Symposium on the Chemistry of Cement. London, 1952. London: Cement & Concrete Association, pp 296–311.

Kersten M, 1996. Aqueous solubility diagrams for cementitious waste stabilization systems. 1. The C-S-H solid-solution system. Environmental Science & Technology, 30, pp 2286–2293.

Kulik D A, Kersten M, 2001. Aqueous solubility diagrams for cementitious waste stabilization systems: II, end-member stoichiometries of ideal calcium silicate hydrate solid solutions. Journal of the American Ceramic Society, 84, pp 3017–3026.

Laaksoharju M, Smellie J, Nilsson A-C, Skårman C, 1995. Groundwater sampling and chemical characterisation of the Laxemar deep borehole KLX02. SKB TR 95-05, Svensk Kärnbränslehantering AB.

Olsson S, Karnland O, 2009. Characterisation of bentonites from Kutch, India and Milos, Greece – some candidate tunnel back-fill materials? SKB R-09-53, Svensk Kärnbränslehantering AB.

Rahman M M, Nagasaki S, Tanaka S, 1999. A model for dissolution of CaO-SiO_2-H_2O gel at Ca/Si>1. Cement and Concrete Research, 29, pp 1091–1097.

Sandström B, Savolainen M, Tullorg E-L, 2004. Forsmark site investigation. Fracture mineralogy. Results from fracture minerals and wall rock alteration in boreholes KFM01A, KFM02A, KFM03A and KFM03B. SKB P-04-149, Svensk Kärnbränslehantering AB.

Sandström B, Tullborg E-L, Smellie J, MacKenzie A B, Suksi J, 2008. Fracture mineralogy of the Forsmark site. SDM-Site Forsmark. SKB R-08-102, Svensk Kärnbränslehantering AB.

SKB, 2006. Long-term safety for KBS-3 repositories at Forsmark and Laxemar – a first evaluation. Main Report of the SR-Can project. SKB TR-06-09, Svensk Kärnbränslehantering AB.

Small J S, Thompson O R, 2008. Development of a model of the spatial and temporal evolution of pH in cementitious backfill of a geological disposal facility. NNL (08) 9601 Issue 4, National Nuclear Laboratory.

Steefel C I, 2008. CrunchFlow: software for modelling multicomponent reactive flow and transport. Berkeley, CA: Earth Sciences Division, Lawrence Berkeley National Laboratory.

Steefel C I, Yabusaki S B, 1996. OS3D/GIMRT: software for multicomponent-multidimensional reactive transport: user's manual and programmer's guide. Richland, Washington: Pacific Northwest National Laboratory.

Sugiyama D, Fujita T, 2006. A thermodynamic model of dissolution and precipitation of calcium silicate hydrates. Cement and Concrete Research, 36, pp 227–237.

Taylor H F W, 1950. Hydrated calcium silicates. Part 1: Compound formation at ordinary temperature. Journal of the Chemical Society, 726, pp 3682–3690.

Walker C S, Savage D, Tyrer M, Ragnarsdottir K V, 2007. Non-ideal solid solution aqueous solution modeling of synthetic calcium silicate hydrate. Cement and Concrete Research, 37, pp 502–511.

Yamamoto T, Imoto H, Ueda H, Hironaga M, 2007. Leaching alteration of cementitious materials and release of organic additives. Study by NUMO and CRIEP, ESDRED. In: R&D on low-pH cement for a geological repository. Proceedings of the 3rd workshop. Paris, 13–14 June 2007, pp 52–61.

Åkesson M, Kristensson O, Börgesson L, 2010. THM modelling of buffer, backfill and other system components. SKB TR-10-11, Svensk Kärnbränslehantering AB.

A.1 Introduction and objectives

In the SKB repository design the use of low-pH cement is envisaged in different situations. In two sub-systems it will be used as structural material: 1) in the tunnel plug, and 2) in the bottom plate.

The function of the low-pH cement in such sub-systems is described below.

A.1.1 Tunnel plug (Figure 1)

The plug has no long term function, but shall be designed so that its sealing function remains until the room or tunnel outside the plug has been backfilled and water saturated, and has regained its hydrostatic water pressure. During the post-operational phase, the plug shall limit water flow from the deposition tunnel past the plug to such an extent that no harmful backfill erosion takes place out from the deposition tunnel.

A.1.2 Bottom plate (Figure 2)

The bottom plate, which consists of a 2 mm thick copper plate on top of a 15 cm thick concrete layer, has only the following two purposes:

- to be a plane, horizontal foundation for the bentonite blocks in the buffer.
- to fasten the temporary bentonite protection (plastic bag and drain tubes before the pellets are installed.

The main objective of the present task is to assess the concrete durability in both sub-systems by means of the chemical degradation process. The durability of the low-pH concrete depends on the geochemical degradation of the mineral phases, during which dissolution can result in increasing the porosity and modifying the permeability of the concrete. These changes can speed up the degradation process and the groundwater flux into the system. Therefore, the concrete durability has to be evaluated by long term reactive transport modelling, accounting for the coupling between dissolution/precipitation of minerals and porosity/diffusivity/hydraulic conductivity changes.

The models to be done should then evaluate quantitatively the long term durability of cementitious components of the repository, including the time evolution of the main physical and chemical properties, and the time evolution of the hydrochemical conditions close to the cementitious components as a result of the hyperalkaline perturbation produced by cement leaching, which can affect the adjacent barriers.

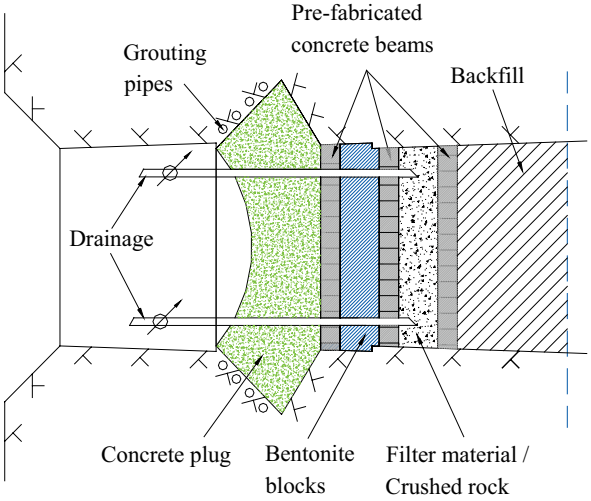

Figure A-1. *Design of the tunnel plug.*

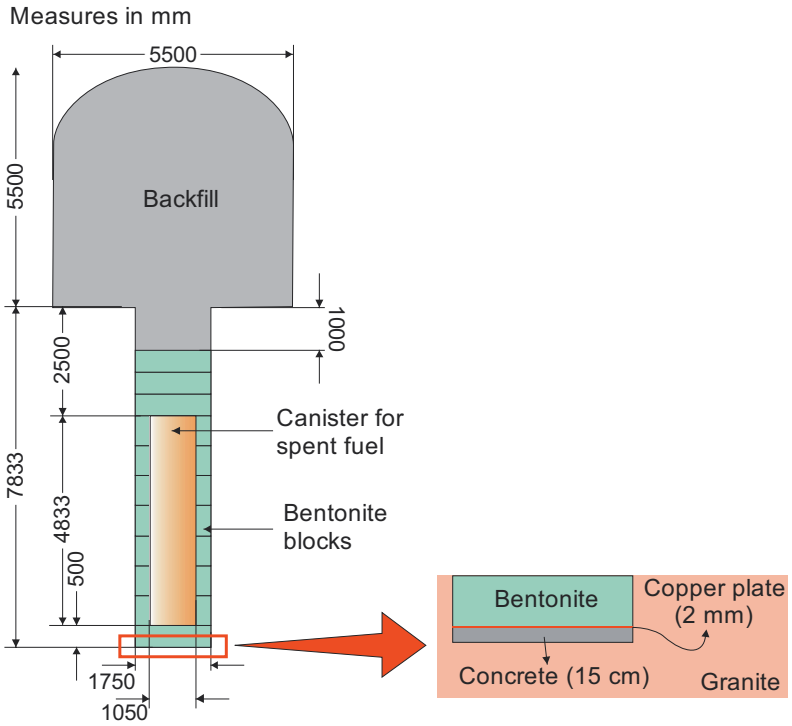

Figure A-2. *Schematic design of the bottom plate.*

A.2 Approach

The approach for the modelling of the low-pH concrete degradation in the tunnel plug and bottom plate sub-systems will be through a reactive-transport model. The methodology that will be used consists of three steps:

1) Simulation of low-pH concrete composition and hydraulic properties.
2) Definition of model domains and cases.
3) Numerical simulation of low-pH concrete degradation in the selected cases.

A.2.1 Step 1: Simulation of low-pH concrete composition and hydraulic properties

The mineral composition of the initial cement paste used for tunnel plug and bottom plate will be calculated. The calculation will be done using the CEMHYD3D /Bentz 2000/ that is a set of computer programs able to simulate the hydration and microstructure development of a three-dimensional arrangement of multi-size, multi-phase concrete particles. The results of this simulation will be used to generate the initial conditions of the subsequent reactive transport models used to simulate the low-pH concrete degradation.

A.2.2 Step 2: Definition of model domains and cases

Although the repository will be located in rock mass of good quality with mostly relatively low fracturing, it can not be disregarded that a hydraulic conductive fracture can be intersected by the low-pH concrete in the tunnel plug and bottom plate sub-systems. The rate of alteration of low-pH concrete is expected to be substantially higher where conductive fractures meet the tunnel plug or bottom plate sub-systems, compared with direct granite-concrete contacts. The evaluation of time evolution of concrete degradation is of importance for SR-Site exercise.

Model domains, cases and scenarios will be carefully analysed and discussed prior to the numerical simulations. The final simulations will be agreed as to ensure that SKB's needs will be fully undertaken in this work.

Possible domains and scenarios to be studied are:

- Degradation of the low-pH concrete plug (and bottom plate) intersected by a vertical (or horizontal) fracture. Under these conditions, a groundwater advective flow will exist in the fracture allowing the concrete – groundwater interaction, allowing concrete degradation by leaching which will increase the porosity and permeability of the concrete.
- A case similar to the previous one but without the presence of a hydraulic conductive fracture. In this case direct contact of the concrete with the granite host rock (and bentonite backfill in the case of tunnel plug) will limit transport of aqueous species to diffusion.

A.2.3 Step 3: Numerical simulation of low-pH concrete degradation in the selected cases

In this step, the durability of the concrete material used in the two sub-systems considered will be quantitatively assessed.

The dissolution and secondary precipitation of the solids in the different components of the system will be considered in the simulations. The solid phases considered as reactive will be selected depending on the final composition of the hydrated paste calculated in the first step. The Calcium-Silicate-Hydrate (CSH) alteration model will be evaluated according to the approach of /Grandia et al. 2010/, i.e. incongruent dissolution-recrystallisation following the /Sugiyama and Fujita 2006/ solid-solution approach. The change of permeability due to porosity change by mineral precipitation/dissolution will be assumed following the Kozeny-Carman relationship, which has been proved satisfactory in this type of problems /Galíndez et al. 2006/.

As the objective of the task is the quantification of the durability of concrete, the total simulation time in the calculations will span depending of the time needed to achieve complete degradation of this material in the simulated problem.

The rate of concrete dissolution is, in part, a function of the Ca and Si concentrations and pH of the inflowing groundwaters. In the simulations, three different groundwater boundary conditions will be used:

1) Groundwater typical of Laxemar site at repository depth.
2) Groundwater typical of Forsmark site at repository depth.
3) Diluted groundwater typical of a glacial case scenario.

Only groundwater from Forsmark has been considered in the model, the reason for that is because Forsmark is the selected site for repository construction and because the main aim is to consider concrete durability during the operational phase of the repository (glacial scenario is not expected during this phase).

The reactive transport models are developed using the CrunchFlow code /Steefel, 2008/ since it is able to handle permeability-porosity dependence issues in addition to other processes as precipitation/dissolution kinetics, solid solutions, and cation exchange.

The main input data for the models are:

- Transport data
  - Groundwater flow through the fracture. This could be obtained by a combination of different parameters (i.e. hydraulic conductivity, hydraulic gradient and hydraulic aperture of the fracture).
  - Diffusion coefficient in granite host rock and bentonite backfill.
  - Hydraulic conductivity and diffusion coefficient of the concrete paste. This is a very important aspect as they will be allowed to change during the calculations due to porosity changes as a function of the dissolution/precipitation process.
  - Bentonite backfill and granite host rock porosity.
- Geochemical data
  - Groundwater composition.
  - Initial water content and composition in cement paste and bentonite backfill. This will be used as initial conditions for the model.

- Initial cement mineral composition. This will be the output of the first modelling step (see above).
- Fracture-filling minerals, especially those that can have an impact on the geochemical evolution of the system.
- Bentonite backfill mineral composition.
- Cation exchange capacity and cation distribution in the bentonite backfill.
- Montmorillonite surface area for protonation/deprotonation reactions.

• Thermodynamic and kinetic data
  - Thermodynamic database, including thermodynamic data for cement minerals.
  - Dissolution – precipitation rates for those minerals present in the system that follow a kinetic law.
  - Cation exchange coefficients.
  - Constants for surface protonation – deprotonation reactions.

In order to fulfil QA requirements the codes CEMHYD3D and CrunchFlow will be qualified according to the SKB procedures including a section in the final report devoted to this qualification.

A.3 Input data

A.3.1 Transport data

Input data needed to simulate groundwater flow through the fracture will be set in order to be in agreement with the $Q_{eq\,1}$ as defined in /SKB 2006/ and /Hartley et al. 2006/. All this data come from the SR-Can assessment and therefore a revision of these data is envisaged as new data are available within the frame of the SR-Site assessment. A value of 5×10^{-6} m^3/yr has been selected for the reference case, although a higher value (5.44×10^{-3} m^3/yr) as that calculated in /Arcos et al. 2006/ will be used as a upper value and to determine the sensitivity of the model to this parameter. However, many deposition holes will not be intersected by any fracture at all and the geochemical evolution will be determined by diffusion alone.

The equivalent groundwater flow rate for $Q_{eq\,1}$ can be written as:

$$Q_{eq\,1} = \sum_f \left(2\frac{Q_f}{\sqrt{a_f}}\sqrt{\frac{4D_w t_{w,f}}{\pi}} \right), \text{ where } t_{w,f} = \frac{L_f \cdot e_{t,f}}{Q_f / \sqrt{a_f}} \qquad \text{(Eq. A-1)}$$

If there are several fractures intersecting a single deposition hole, then a conservative approach to calculate the equivalent groundwater flow-rate requires the flow to be summed across all the fractures. Hence, the equivalent Darcy velocity, U_{r1}, for all fractures intersecting the deposition hole is:

$$U_{r1} = \frac{1}{w_c}\sum_f \frac{Q_f}{\sqrt{a_f}} \qquad \text{(Eq. A-2)}$$

where:

D_w is the diffusivity in water, [m^2/yr],

$t_{w,f}$ is the time the water is in contact with the deposition hole within each fracture, [yr],

L_f is the length of the fracture intersection with the wall of the deposition hole, [m],

U_{r1} is the average initial Darcy velocity in the fracture system averaged over the rock volume adjacent to the canister (water flux) [m/yr],

Q_f is the volumetric flux in the fracture adjacent to the deposition hole [m^3/yr],

$e_{t,f}$ is the transport aperture of the fracture adjacent to the deposition hole [m],

a_f is the area of the fracture plane intersecting the hole [m^2],

w_c is the canister height [m].

The following data have been selected in order to calculate the needed input parameters for the model.

Parameter	Value	Units	Source
w_c	5.0	m	/Hartley et al. 2006/
L_f	5.5	m	Calculated from KBS-3 design
U_{r1}	10^{-5}	m/yr	/SKB 2006/
Fracture thickness	0.116	m	/Arcos et al. 2006/ /Dershowitz et al. 2003/
D_w	2.8×10^{-10}	m^2/s	/Arcos et al. 2006/

With these data values the following parameters can be calculated:

$a_f = 0.6377\ m^2$

And according to Equation A-2:

$$Q_f = U_{r1} \cdot w_c \cdot \sqrt{a_f} = 3.99\times10^{-5}\ m^3/yr \qquad \text{(Eq. A-3)}$$

The input parameters for the transport in the fracture are: the porosity (ε), the fracture thickness, the diffusion coefficient in water (D_w), the hydraulic conductivity (K), and the hydraulic head gradient (i). A value for K of 5×10^{-10} m/s has been selected according to /Follin et al. 2005/, which allows to calculate the hydraulic gradient ($i = U_{r1}/K$) . Therefore, as fracture thickness, D_w, K, and i are fixed values, the only input parameter that needs to be calculated is porosity (ε). From Equation A-1, the value of $t_{w,f}$ to obtain a $Q_{eq\ 1}$ of 5×10^{-6} m^3/yr is 4.46 years, and therefore the $e_{t,f}$ has to be 4.06×10^{-5} m. Assuming that $e_{t,f}$ is the fracture thickness times the porosity, then the calculated porosity is 0.00035, which is in agreement with the porosity values from Äspö /Dershowitz et al. 2003/.

As the important parameter in the model is the groundwater flow for advective transport through the fracture, any relationship of porosity (ε),hydraulic conductivity (K) and hydraulic head gradient (i), resulting in the target $Q_{eq\ 1}$ value could be valid. Therefore, for the extreme case, where $Q_{eq\ 1}$ is taken as 5.44×10^{-3} m^3/yr /Arcos et al. 2006/, the following parameters have been modified:

$U_{r1} = 0.11$ m/yr

$i = 0.688$

Effective diffusivity (D_e) for the four system components (concrete, bentonite backfill, fracture, and granite host rock) will be discussed and selected.

Other transport input data, as hydraulic conductivity and porosity of bentonite backfill, will be the same as selected in /Arcos et al. 2006/, and indicated in the following table.

	Backfill (IBECO-RWC-BF)
K (m/s)	10^{-12}
Porosity	0.45

As previously indicated, all the data will be revisited in the frame of the SR-Site assessment as far as new transport data are available in order to gain coherence with other tasks developed within SR-Site.

A.3.2 Geochemical data

The most relevant data needed for the simulations of this project are: (1) the cement recipe in order to simulate the cement hydration processes and (2) the chemical properties of the groundwater used as boundary conditions in the cement degradation models.

Concerning the cement recipe, these data will be requested from the appropriate persons in SKB. The information about the cement recipe will be taken from the "underground opening construction report". Draft version of this report is now in the process of being finalized.

For groundwater compositions, in the following table those used in /Arcos et al. 2006/ are presented. However, new groundwater compositions with their corresponding uncertainties will be delivered by SKB, and therefore, as for the case of transport data, the new data will be used for the calculations in order to gain coherence with other tasks developed within SR-Site.

moles/L	Forsmark	Laxemar saline[1]	Grimsel Ice-melting
pH	7.2	7.9	9.6
pe	–2.42	–5.08	–3.38
HCO_3^-	2.20×10^{-3}	1.00×10^{-4}	4.50×10^{-4}
Ca	2.33×10^{-2}	4.64×10^{-1}	1.40×10^{-4}
Cl	1.53×10^{-1}	1.28	1.60×10^{-4}
Fe tot	3.31×10^{-5}	8.00×10^{-6}	3.00×10^{-9}
K	8.75×10^{-4}	7.00×10^{-4}	5.00×10^{-6}
Mg	9.30×10^{-3}	1.00×10^{-4}	6.20×10^{-7}
Na	8.88×10^{-2}	3.49×10^{-1}	6.90×10^{-4}
SO_4^{2-}	6.80×10^{-3}	9.00×10^{-3}	6.10×10^{-5}
Si	1.85×10^{-4}	8.00×10^{-5}	2.05×10^{-4}

[1] Data for saline water as reported in /SKB 2006/, except for pe and silica, which come from /Laaksoharju et al. 1995/.

Fracture-filling minerals in the geosphere will be obtained from /Sandström et al. 2004/ and /Sandström et al. 2008/ whereas mineral composition, as well as CEC and montmorillonite surface area data of bentonite backfill will be those reported in /SKB 2006/ which are equivalent to those used in /Arcos et al. 2006/.

For concrete, the composition of the hydrated cement is calculated from the recipes provided by the manufacturers. In Section 4, details of the methodology used and results are provided.

A.3.3 Thermodynamic and kinetic data

We will use the thermodynamic database from SKB's Trac system. Thermodynamic and kinetic data for cement minerals will be discussed and selected.

A.4 Software list and handling of configuration and scripting files

A.4.1 CEMHYD3D

This tool is provided by the Virtual Cement and Concrete Testing Laboratory (VCCTL; http://ciks.cbt.nist.gov). The main underlying program of the VCCTL, namely CEMHYD3D, was developed by /Bentz et al. 1994/ and was intensively tested in numerous applications /Bentz 1997/, /Bentz and Haecker 1999/, /Bentz et al. 1999/, /Bentz et al. 2000/, /Bentz and Conway 2001/.

The simulation of cement hydration would involve the use of SEM (Scanning Electron Microscopy) images of the un-hydrated cement materials in question. Since such images are not available in our case, some hypotheses should be made during the course of the analysis.

The process of numerical generation of the final microstructure of the hardened cement proceeds in a series of steps: (1) the creation of the particle size distribution for both cement clinker and silica fume; (2) the generation of the initial microstructure; (3) the distribution of cement phases and (4) the simulation of hydration.

By creating a particle size distribution (i.e. the mass fraction expressed as a function of particle diameter) the number of cement particles of each diameter to be placed in a starting three-dimensional microstructure is specified. Two different input (PSD) files are generated, one corresponding to the anhydrous cement itself, and the other to the silica fume added.

The volume (or the number of pixels in a three-dimensional image of the mixture) assigned to each compound must be adjusted by using available values in the simulated recipe, in order to match the prescribed water-to-cement ratio for each mix design.

A three-dimensional cement-based mixture microstructure is then generated, consisting of the sum of the selected compounds in water, namely cement clinker and, when available, silica fume, with their respective particle size distribution. The influence of the superplasticizer can also be modelled in a two-fold way: by enabling the flocculation into several flocs; and by 'dispersing' the particles into the initial microstructure. Details of the process can be found in the User's Guide of CEMHYD3D /Bentz 2000/.

Since the microstructure image created by the preceding steps is composed of single-phase particles only, once the initial arrangement of generic anhydrous particles in water has been created, the four major phases of cement clinker (i.e. C_3S, C_2S, C_3A and C_4AF) should be distributed amongst the cement particles.

Ideally, the three-dimensional microstructure image is filtered using two-point correlation functions measured on the actual two-dimensional SEM images of the cement in question. Once the anhydrous mixture was sketched, the numerical simulation of the hydration process is performed by CEMHYD3D.